Study of the characterization and therapeutic effect of fluorescent anti-fibrotic extracellular vesicles

Danielle Novillo Quirola

Master's Degree in Biomedicine and Molecular Biology

Instituto de Biomedicina y Biotecnología de Cantabria (IBBTEC)

Director: Dr. Ana Victoria Villar Ramos

2020-2021

Acknowledgments

First thank God for his blessings and protection, as well as my parents for being my strength, also for their unconditional and immense love for me. I would like to thank the University of Cantabria for the opportunity to learn from the best professors and researchers, furthermore to IBBTEC for letting me use the different laboratories and equipment for the development of this work. I thank to my tutor, Dr. Ana Villar for believing and giving me the chance to join her group and treating me like one of them, in the same way I thank Dr. Ana Palanca for her help. To all the members of the research group of which I was part of, especially I want to thank Jorge, for having been very patient teaching, guiding, and helping me in this learning process and above all for starting as my supervisor and ending up being my friend, giving me his support and sharing thousands of laughs. Thanks to David, Luis, Elena and Mariadel for their friendship and shared moments. And to my roommate Nor for all the time spent together in which she always showed me her support and motivated me to keep going.

Table of Contents

1. State of art 1

Cardiac Fibrosis 1

TGF β role in cardiac fibrosis 3

Hsp90 4

Anti-fibrotic therapy: cTPRAu-390 5

Extracellular vesicles as biotherapeutic molecules and nanocarriers for drug delivery 5

2. Objectives 9

3. Materials and methods 10

Isolation of extracellular vesicles 10

Cell culture 10

EVs isolation protocol 10

Characterization 11

Electron microscopy Negative Staining 11

Dynamic Light Scattering 11

Flow cytometry 11

Western blotting 11

cTPRAu-390 encapsulation into EVs 12

Flow cytometry analysis to detect the encapsulation of the therapy into EVs 13

Different treatments for analyzing profibrotic gene expression in NIH-3T3 cells. 13

Study of gene expression of the genes of interest 14

RNA isolation 14

Reverse Transcription 15

Real time PCR (qPCR) 15

EVs internalization assay 16

Fluorescence microscopy assays to visualize the internalization of EVs into cells 16

Confocal microscopy assays to detect internalized EVs 17

Fibrotic mice generation 17

In vivo imaging system experiments to visualized EVs distribution in different organs in a fibrotic mouse 17

4. Results 18

Protein concentration of NIH-3T3-derived EVs 18

EVs characterization 18

1. Diameter of EVs 18
2. Charge measurement of EVs 20
3. Analysis of the number of EVs per sample 21

4. Detection of EVs markers 22
Analysis of the encapsulation of cTPRAu-390 into EVs 24
Genes expression analysis 25
Detection of EVs internalization 26
EVs distribution in fibrotic mice through *in vivo* imaging and after EVs administration 32
5. Discussion 36
6. Conclusions 40
Bibliography 41

1. State of art

Cardiac Fibrosis

Cardiovascular diseases (CDV) are one of the most severe disorders and cause of death worldwide, are a rapidly arising problem in industrialized and developed countries (Henderson et al., 2020). World Health Organization mentioned that around 17.9 million people die of CDV each year mainly from heart attack and stroke, accounting for 30% of all global deaths. By 2030, nearly 23.6 million people might die from CDV, remaining the leading cause of death (WHO, 2017). Almost in all cardiovascular diseases such as hypertension, myocardial infarction, and aortic valve stenosis (Fang et al., 2017) appears a common hallmark, cardiac fibrosis (Biernacka & Frangogiannis, 2011). Fibrosis is not a disease (Henderson et al., 2020), initially acts as a beneficial process of repaired but the maladaptive response to injury develops the accumulation of extracellular matrix components, mainly collagen (Murtha et al., 2017) producing chamber dilation and hypertrophy as pathological changes at the injured tissue (Lu et al., 2017; Murtha et al., 2017); as a result, the size of the fibrotic tissue is expanded, thus causing cardiac function disease and cardiac death (Ding et al., 2020; Z. Fan & Guan, 2016).

Different cell types are found in the heart (Nandi & Mishra, 2015) three main types related to the number of cells are cardiomyocytes known commonly as heart cells, endothelial cells, and fibroblasts (Talman & Ruskoaho, 2016). Pinto et al., 2016 study revealed that cardiomyocytes and endothelial cells are the most abundant cell type in relation to fibroblasts that represent the third part of cardiac cellular composition (**Figure** 1). In the myocardium are present three types of collagen fibers, type I, III and IV being the main fibers type I (80%) and III (10%) (Gallego Muñoz et al., 2019).

It is known that fibrotic response is mainly activated by cardiac fibroblasts (Aujla & Kassiri, 2021). Cardiac fibroblasts (cFBs) are flat, spindle-shaped (Gibb et al., 2020; Tian et al., 2017) mesenchymal cells origin and main producers of extracellular matrix to maintain a normal cardiac environment; therefore act as regulator cells to keep homeostasis of the extracellular matrix (ECM) which acts as a scaffold for cardiac cells (DeLeon-Pennell et al., 2020) in addition, are involved in structural, mechanical, and electrical cardiac function.

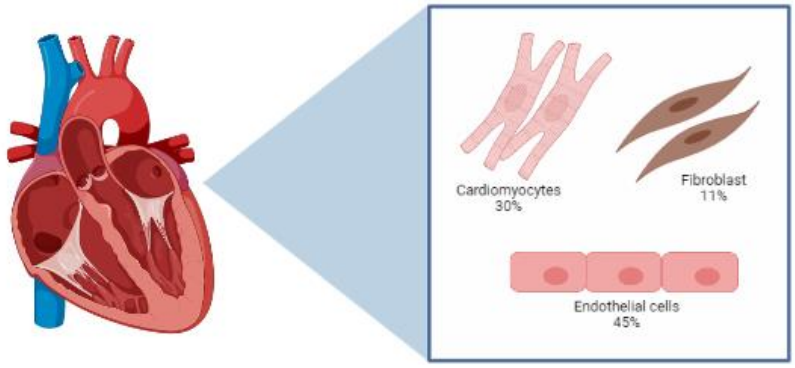

Figure 1. Most abundant cardiac cell types and its percentage of abundance in heart (Pinto et al., 2016).

Activation of cFBs starts with a pathological stimulus which trigger a profibrotic signaling having as result an excess of ECM proteins, this stimulation can be done by different signaling such as cytokines, renin angiotensin system and others (Ranjan et al., 2019). It is known that the major signaling effector of cFBs transdifferentiation into myofibroblasts (myoFBs) is the cytokine TGF β. Myofibroblasts transdifferentiation consists of two stages: the first stage consists of the adhesion of the complexes followed by the formation of stress-fiber network that helps the migration of proto-myofibroblast to the affected tissue; while in the second stage proto- myofibroblasts become mature myofibroblast which secrete alpha-smooth muscle actin (α-SMA) protein (Yousefi et al., 2020) known as the main marker of myofibroblasts (Parichatikanond et al., 2020). Mature myofibroblast produce an excessive amount of extracellular matrix proteins such as collagen I, III, IV, fibronectin and a different type of cytokines (Yousefi, et al., 2020); in addition the development of scar tissue (**Figure** 2) (Leask, 2015). Moreover, activated fibroblasts also overexpress ECM components been involved in the profibrotic process under TGF β stimulus (Melzer et al., 2020).

The action of fibroblasts can produce different types of fibrosis. It should be mentioned that the classification of cardiac fibrosis depends on the place and cause (Fan et al., 2012) but, reactive interstitial and reparative fibrosis are the most common (Murtha et al., 2017). Interstitial fibrosis is the process of cardiomyocyte replacement (Ranjan et al., 2019) due to the activation of fibroblasts responsible for degrading the stroma and depositing excess ECM proteins, hindering the contractile capacity of the myocardium (Aujla & Kassiri, 2021); on the other hand, replacement fibrosis is a process of repair (Murtha et al., 2017) in which lost cardiomyocytes are re-emerged with collagen scars (Ranjan et al., 2019) to maintain the myocardial structure (Aujla & Kassiri, 2021).

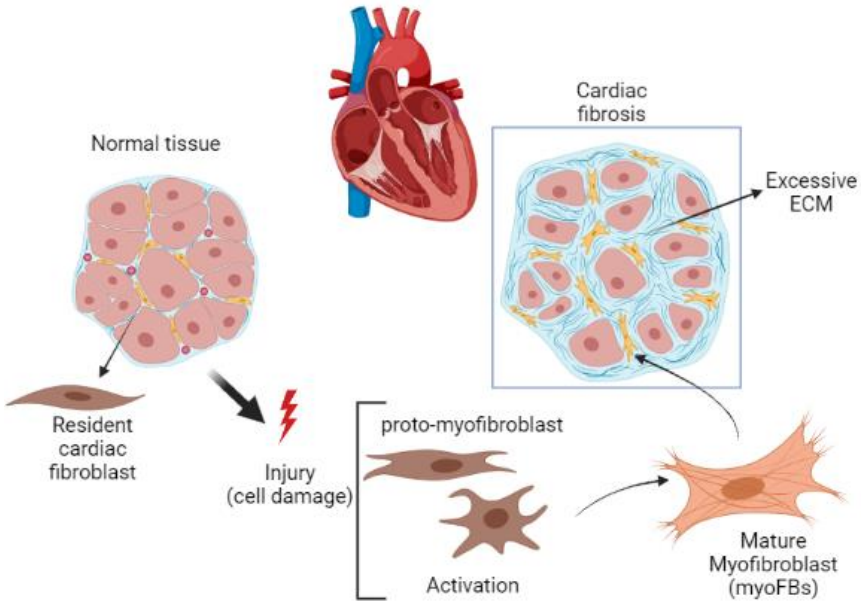

Figure 2. Scheme of one of the two ways of activation of fibroblast in development of cardiac fibrosis. Created with Biorender.com

TGF β role in cardiac fibrosis

Studies have demonstrated that the cytokine transforming growth factor β (TGF-β) is the major contributor in the activation of fibrotic responses (Leask, 2007) specially triggers the overexpression of ECM compounds during cardiac fibrosis (Ma et al., 2018). Three isoforms of TGF β have been identified (TGF β1, TGF β2 and TGF β3) encoded by three different genes (Ma et al., 2018) and secreted by many types of cells, for example macrophages and damaged cardiomyocytes (Liu et al., 2017). Studies have described TGF β1 as the most prevalent isoform implicated in fibrosis and found in mammalian tissues (Biernacka et al., 2011). TGF β is involved in the activation of fibroblasts and in the transformation of fibroblasts into myofibroblast once it binds to its type I and II receptors and to TGF β/Smad signaling (Liu et al., 2017).

The cytokine TGF β is present in a healthy heart as a latent complex retained in the ECM (Kong et al., 2014; Parichatikanond et al., 2020), it is composed by three proteins such as TGF β, latency associated peptide (LAP) and latent TGF β binding proteins (LTBPs) which prevents it from binding to its receptors (Yousefi et al., 2020). Excess TGF β causes the change from a latent complex to an active form by binding to its receptor being released from ECM (Kong et al., 2014); a signaling cascade is initiated by the binding of TGF β to its heterodimeric transmembrane receptors type I (TGFβR1) and type II (TGFβR2) interceded mainly by Smad cell mediators in the canonical route of signaling (Parichatikanond et al., 2020).

TGF β type I receptor is a serine-threonine kinase, also named activin linked kinase 5 (ALK5) (Leask, 2015). In the canonical pathway in the presence of TGF β ligand, this receptor assists in the phosphorylation of Smad2 and 3. Phosphorylated Smad2/3 proteins binds to Smad 4 (mediator Smad) forming a heteromeric complex followed by a nuclear translocation to activate gene expression of pro-fibrotic genes such as collagens and fibronectin (Gibb et al., 2020; Parichatikanond et al., 2020; Yousefi et al., 2020) (**Figure** 3).

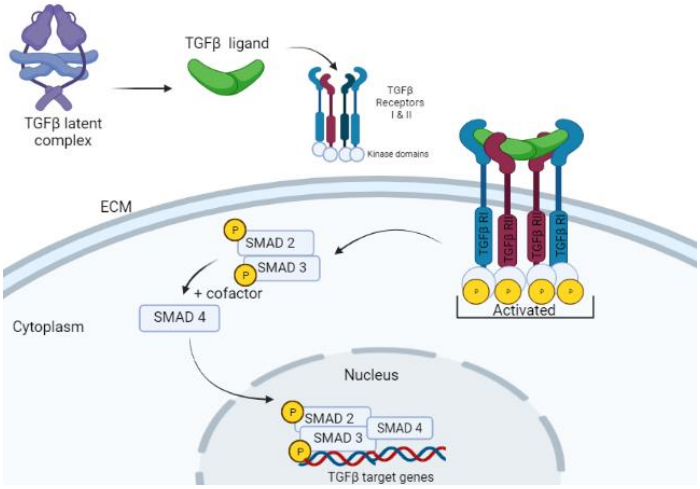

Figure 3. Scheme of canonical pathway of activation of TGF β (Parichatikanond et al., 2020). Created with BioRender.com.

TGF β activates other non-canonical pathways which include mitogen-activated protein kinases (MAPK) pathways such as c-Jun- N-terminal (JNK), extracellular signal-regulated kinase (ERK) and p38 MAPK, phosphatidylinositol 3 kinase (PI3K) and Rho-like GTPases (Biernacka et al., 2011; Finnson et al., 2020; Travers et al., 2016).

TGF β signaling cascade presents several mediators and partners helping the efficiency of profibrotic protein expression. Those mediators are potential targets to reduce fibrosis due to blocking TGF β causes important side effects in patients. One such mediators is known to be heat shock 90 chaperone (Hsp90), the absence of which reduces collagen expression *in vitro* and *in vivo* by participating at plasma membrane level as well as intracellularly (Cáceres et al., 2018) in cardiac fibrosis models.

Hsp90

Heat shock protein 90 (Hsp90) is a molecular chaperone and one of the main and the most studied heat shock proteins (HSPs) with a molecular weight of 90 kDa (Colunga Biancatelli et al., 2020; Hoter et al., 2018). There are four types, Hsp90 α (I &II) and Hsp90 β are in the cytoplasm whereas GRP94 in endoplasmic reticulum (ER) and TRAPI in the mitochondria (Hoter et al., 2018; X. Zhang et al., 2021); being the main ones Hsp90 α and β (Zhang et al., 2021). Hsp90 is involved in processes of stabilization of TGF β receptors (Cáceres et al., 2018; Hoter et al., 2018; Tomcik et al., 2014; Wrighton et al., 2008). It is known that fibroblasts and some other cell types secrete Hsp90 in small amounts (Hoter et al., 2018), this extracellular Hsp90 forms a complex with the TGF β1 receptor thus enabling TGF β to bind to its receptor triggering ECM compounds gene expression (García et al., 2016; X. Zhang et al., 2021). Therefore, different studies showed that in fibrotic diseases Hsp90 inhibitors such as 17-AAG, 17-DMAG, geldanamycin, radicicol and other new therapeutic strategies can reduce fibrogenesis by inhibiting Hsp90 and blocking TGF β1 signaling cascade, thus ECM synthesis (Cáceres et al., 2018).

Tomcik et al., 2014 study demonstrated that Hsp90 inhibition suppresses profibrotic effects and revealed that 17 DMAG inhibitor avoid the accumulation of the phosphorylated Smad2/3 complex in the nucleus, preventing fibroblast transdifferentiation into myofibroblast. Also, in García et al., 2016 study was demonstrated that inhibition of extracellular Hsp90 leads to a reduction in collagen I expression in TGF β-activated mouse embryonal fibroblasts. As well as Cáceres et al., 2018 study that showed a decreased of collagen expression in myocardial fibrosis using an engineered fluorescent-labeled Hsp90 protein inhibitor named CTPR-488 which breaks into TGF β/Hsp90 complex. Furthermore, in Solopov et al., 2019 study was validated that Hsp90 inhibitor AUY-922 prevents the development of chronic lung injury and pulmonary fibrosis by exposure to nitrogen mustard. In the same way in Marinova et al., 2020 study was used Hsp90 inhibitor AUY-922 in treatment of chronic lung injury and pulmonary fibrosis but given by exposure to HCl, same way they confirmed the efficiency of this inhibitor blocking adverse effects. Colunga Biancatelli et al.,

2020 used Hsp90 inhibitors to modulate proteome involved in idiopathic pulmonary fibrosis (ipf) by interfering with TGF β (Smad and non Smad) intracellular signaling.

All these results point to Hsp90 as a good target to reduce fibrosis. The design of new therapies that maintain the chaperone activity of Hsp90, and thus cellular homeostasis, while reducing the ability of Hsp90 to interact with TGF β signaling mediators, seems to be a good therapy in fibrotic diseases.

Anti-fibrotic therapy: cTPRAu-390

The engineered tetratricopeptide repeat scaffold (TPR) are protein domains mediating protein-protein interactions and present in different proteins (Cortajarena et al., 2010; Perez-Riba & Itzhaki, 2019). It consists of 34 amino acids of 2 to 20 repeats giving a coiled and superhelical shape (Perez-Riba & Itzhaki, 2019). Taking this domain as scaffold, our collaborators at CIC-BiomaGune generated nanoclusters based on non-functional TPR modules bind to a functional TPR that specifically binds Hsp90.

We named this nanocluster construction cTPRAu-390 nanocluster, and it can inhibit cardiac fibrosis by blocking TGF β signaling pathway *in vitro* and *in vivo* (Cáceres et al., 2018). Because the functional TPR binds to C-terminal Hsp90 region causing a change in its conformation and releasing TGFβRI thus inhibiting fibrosis but without affecting its ATPase function (**Figure** 4), also gold molecules were conjugated to confer the nanocluster fluorescence becoming a theragnostic tool that is able to localize the injury and treat it (Aires et al., 2021; Cáceres et al., 2018). To improve the *in vivo* biodistribution of the nanocluster and to avoid the first hepatic step if it happens, we want to use a biocompatible vehicle as drug delivery.

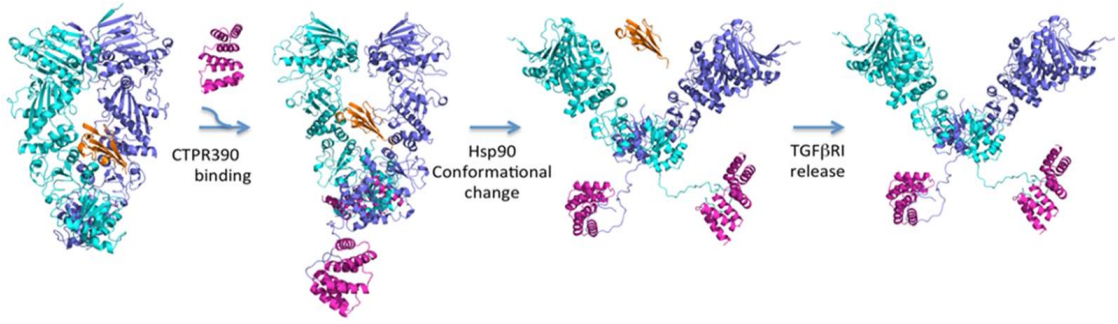

Figure 4. Scheme of the molecular model of interaction of Hsp90 (cyan and dark blue) with the nanocluster cTPRAu-390 (violet) and its conformational change that triggers the release of TGFβRI (orange) (Cáceres et al., 2018).

Extracellular vesicles as biotherapeutic molecules and nanocarriers for drug delivery

Cell-to-cell communication is essential in all multicellular organisms. This process is given by emission of different type of signals, nowadays it is known that this communication can also be carried out by biological complexes called extracellular vesicles (Tkach & Théry, 2016). International

Society for Extracellular Vesicles (ISEV) defines extracellular vesicles (EVs) as nanoparticles released by cell and composed of a lipid bilayer membrane without functional nucleus and not able to replicate (Théry et al., 2018), carrying active biomolecules such as RNAs, proteins and lipids (Tkach & Théry, 2016), initially were though that they were secreted for the removal of unnecessary compounds from the cell, but nowadays it is known that EVs are more than just a waste (Van Niel et al., 2018); they are able to transport cargo to the recipient cell (Zaborowski et al., 2015) making them important regulators in cell to cell communication diagnostic tools and as drug delivery vehicles (Boulanger et al., 2017; El Andaloussi et al., 2013). Extracellular vesicles are secreted by all cell types and can be found in bodily fluids such as urine, blood, and saliva (Doyle & Wang, 2019; Ha et al., 2016; Théry et al., 2018).

ISEV has suggested that EVs can be classified according to the following features: physical characteristics such as size, chemical composition, and the quantity of charge on their surface (Gandham et al., 2020). Based on their intracellular origin exist three types of extracellular vesicles: microvesicles, exosomes and apoptotic bodies (Ha et al., 2016).

Microvesicles are originated by directly budding and fission of the plasma membrane (Zaborowski et al., 2015). ADP-ribosylation factor 6 (ARF6) is responsible for initiating the signaling cascade via phospholipase D (PLD) activation which engages extracellular signal- regulated kinase (ERK) binding to the plasma membrane, and this kinase activates the phosphorylation of myosin light-chain kinase (MLCK) triggering the release of microvesicles (**Figure** 5) (Akers et al., 2013) with a ranging size 100 nm to 1 μm (Van Niel et al., 2018). Due to the method by which microvesicles are obtained, they contain transmembrane proteins as tetraspanins (CD9, CD63, CD81 & CD82), another found are cytoskeleton proteins (Actin, tubulin), heat shock proteins, integrins involved in the attachment to target cells and proteins with post transcriptional modifications (Doyle & Wang, 2019).

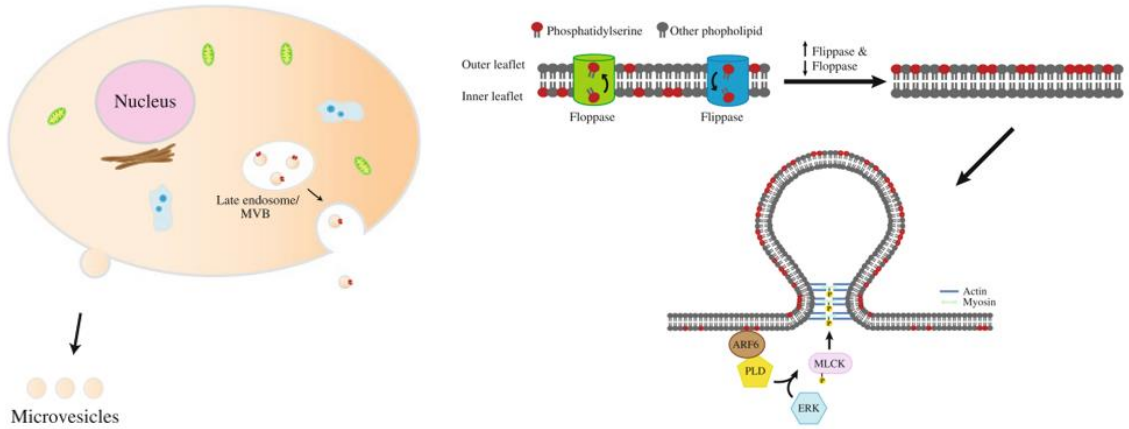

Figure 5. Biogenesis of microvesicles by budding and fission of plasma membrane (Akers, 2013). ARF: ADP-ribosylation factor 6, PDL: phospholipase D, ERK: extracellular signal- regulated kinase; MLCK: myosin light-chain kinase.

In the other hand, exosomes are smaller than microvesicles with a ranging size from 40 to 130 nm, are formed from the endosomal pathway. Multivesicular bodies (MVBs) developed from early endosomes. By inward budding of the multivesicular bodies intraluminal vesicles (ILVs) are formed inside MVBs. MVBs fusion with the plasma membrane, release ILVs outside the cell becoming exosomes (**Figure** 6)(Akers et al., 2013; de Abreu et al., 2020; Yáñez-Mó et al., 2015). It is known that endosomal sorting complex required for transport (ESCRT) is involved in the formation of ILVs which is an intricate protein composed of four proteins (0, I, II & III); furthermore, ESCRT mechanism is triggered by the identification and attachment of ubiquitinated proteins to endosomal specific membrane domains through the ESCR-0 ubiquitin-binding subunits that interact with ESCRT-I and ESCRT-II complexes, and this complex combines with ESCRT-III complex (involved in the budding process). Finally, after buds are cleaved to form ILVs, sorting protein Vsp4 provides energy necessary for ESCRT-III complex detachment from MVB membrane (Zhang et al., 2019). ESCRT-III is thus recruited to the ESCRT-I and II site by the Alix protein, which binds simultaneously to TSG101 component of the ESCRT-I complex and to charged multivesicular body protein 4 (CHMP4), ESCRT-III component (Akers, et al., 2013). Following proteins are part of exosomes composition: tetraspanins such as CD9, CD63 & CD81; major histocompatibility complex II (MCHII); membrane transport & fusion proteins (Annexins, Flotillin-1, Syntenin-1 & GTPases); cluster of differentiation (CD); heat shock proteins (Hsps); Ras related protein (Rab); adhesion molecules known as integrins and other such as TSG101, Hsp90 β, Syntenin-1 & Allix embedded into exosomes after its formation (**Figure** 7) (Doyle & Wang, 2019; Zaborowski et al., 2015). However, there is still a lack of specific markers to differentiate microvesicles from exosomes (Doyle & Wang, 2019).

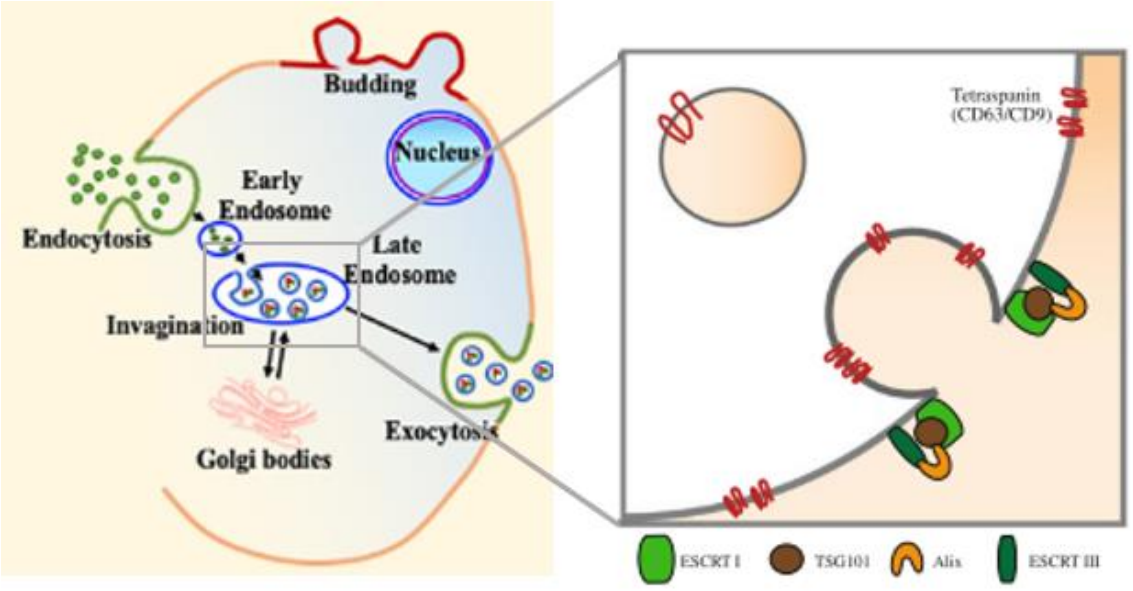

Figure 6. Scheme of exosomes biogenesis and its different types of compounds. Exosomes carry cellular components DNA, miRNA, mRNA, and intracellular proteins such as tetraspanins, Allix and TSG101 (modified of Ha et al., 2016; Ranjan et al., 2019).

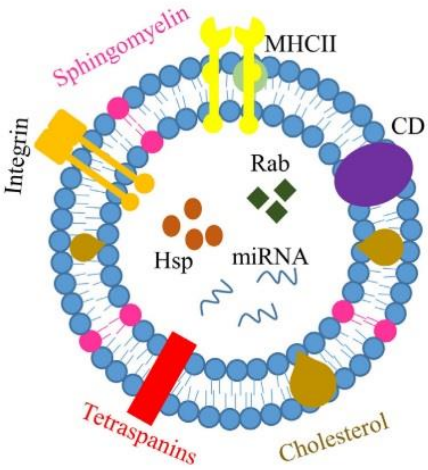

Figure 7. Scheme of various exosomes components such as MHCII: major histocompatibility complex II, CD: cluster of differentiation, Rab: Ras-related, Hsp: heat shock proteins, tetraspanins, etc.; it also contains different type of lipids as cholesterol, sphingomyelin. Exosomes contain nucleic acid including miRNA. (Ha et al., 2016).

Finally, during apoptosis the cells are reduced and fragmented into apoptotic bodies (**Figure** 8), having a ranging size from 0.5 to 2 μm (Janas et al., 2015) are release by dependent on Rho associated kinase I (ROCK) with ATPase activity (Sluijter et al., 2014). The presence of organelles inside the vesicles is what defines them (Van Dommelen et al., 2012) it also contains glycosylated proteins and chromatin (Doyle & Wang, 2019).

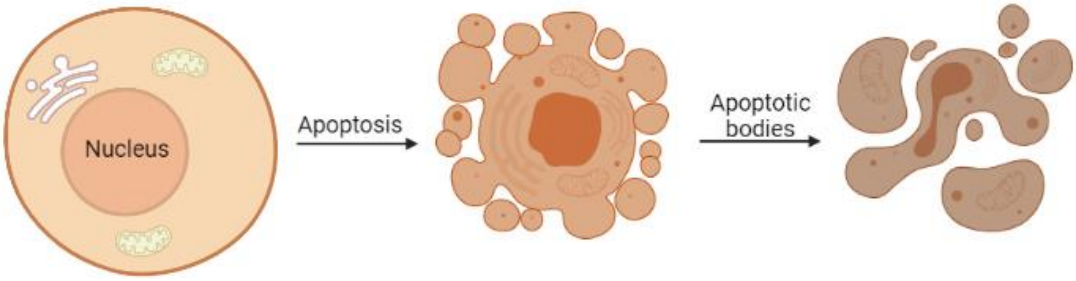

Figure 8. Development of apoptotic bodies during apoptosis. Created with Biorender.com

Exosomes and microvesicles are similar in their appearance, overlap in sizes and are often common in composition, which makes it difficult to identify their origin upon isolation from biological fluids or extracellular medium (Van Niel et al., 2018).

It seems that EVs can carry different cargoes such as lipids, proteins, and nucleic acids. Extracellular vesicles will exhibit a set of cell type-specific proteins that account to their specific targets and roles (**Figure** 9) (Van Niel et al., 2018).

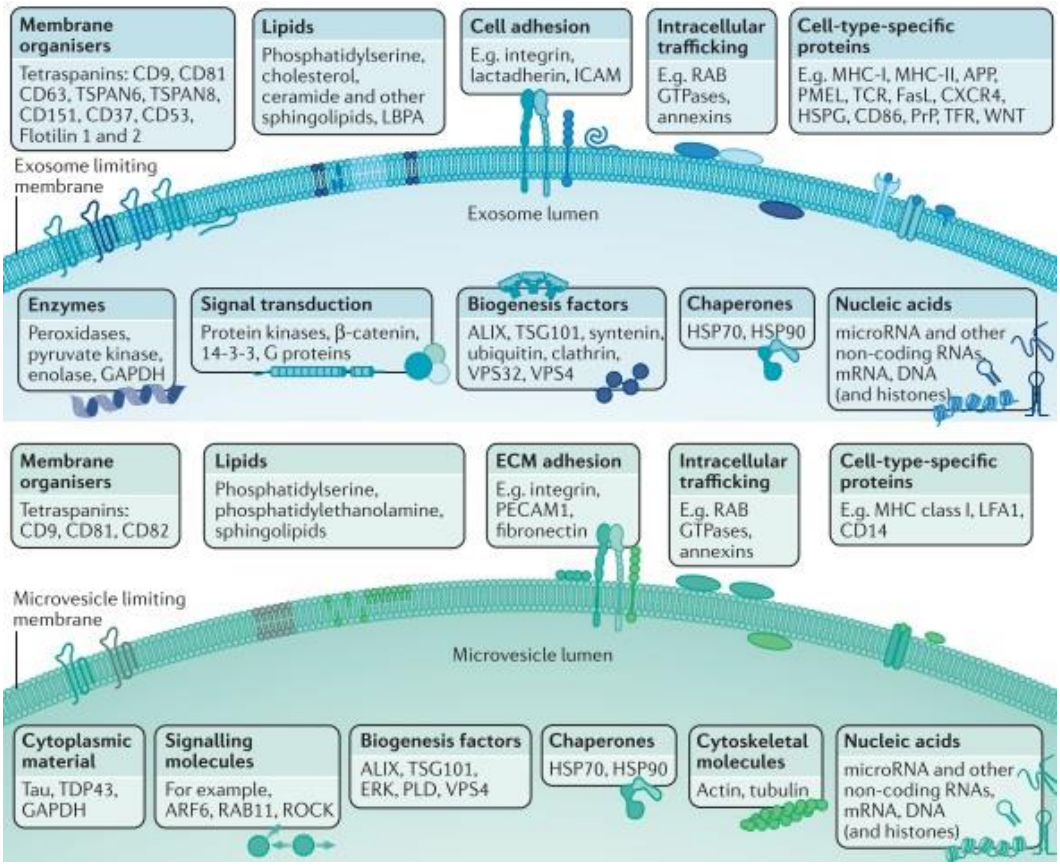

Figure 9. Different biomolecules carried by exosomes and microvesicles (Van Niel et al., 2018).

de Abreu et al., 2020 study mentioned that an important feature of extracellular vesicles is their negative surface charge, therefore nanoparticles near neutral charge are most stable in the circulation in comparison to highly charged nanoparticles.

Extracellular vesicles are ideal as drug delivery vehicle due to their long circulating half-life, biocompatibility being well behave by human organism, inherent capacity to target tissues, in addition is capable to be internalized into the cell, also can act as a therapeutic tool and present minimal or no implied toxicity (Doyle & Wang, 2019; Ha et al., 2016).

The vesicles of interest in this study are microvesicles and exosomes due to their capacity of cell carriers without immune response and their high potential of carrying the desired drug-cargo.

2. Objectives

This study has six objectives:

1. Purification of the extracellular vesicles from NIH-3T3 fibroblasts.
2. Characterization of EVs by electron microscopy, dynamic light scattering, flow cytometry and western blotting technique.
3. Analysis of the expression of the main profibrotic genes (Col I, Col III and Fibronectin) after microvesicles administration to NIH-3T3 cells.

4. Evaluation of EVs encapsulation with a therapeutic strategy and analysis of the expression of the main profibrotic genes (Col I, Col III and Fibronectin) after their administration in NIH-3T3 cells.
5. Verification of the internalization of encapsulated and non-encapsulated EVs in NIH-3T3 cells.
6. Observation of *in vivo* distribution in a fibrotic model mouse of fluorescent EVs.

3. Materials and methods

Isolation of extracellular vesicles

Cell culture

Mouse embryonal fibroblasts NIH-3T3 cell line was used in this study. Cells were cultured in Dulbeco Modified Eagle's Medium High Glucose (DMEM) supplemented with 10% Fetal Bovine Serum (FBS) and 1% penicillin- streptomycin. Cultured conditions were 37°C 100% of humidity and 5% of CO_2 using Thermo Scientific Forma 381 Steri Cycle CO2 Incubator. We also used a stable fluorescent cell line 3T3 mKATE created in our group that express the fluorescence protein mKATE 2 binds to all cell membranes, which also confers fluorescence to the EVs released by these cells.

EVs isolation protocol

Fourteen 150 mm plates with NIH-3T3 cells at 75% confluence were used, cells were washed with PBS and cultured for 5 days without EVs supplementing the medium with EVs depleted FBS. Then, the medium containing EVs released from NIH-3T3 cells was collected to start the isolation.

Since the size between microvesicles and exosomes differs from each other, there are different methods for the isolation of extracellular vesicles, the most used technique being the differential centrifugation (Zaborowski, Balaj, Breakefield, & Lai, 2015). First, to eliminate cellular debris and death cells was done a first centrifugation, carried out at 2000 × g for a time of 30 minutes, then supernatant was transferred to polyallomer tubes correctly calibrated to be used in an AH29/36 rotor (Thermo Scientific Sorvall). A first ultracentrifugation was performed at 10,000 × g for 90 minutes to pellet the microvesicles. The supernatant was ultracentrifuged at 100,000 × g for 90 minutes to pellet exosomes. Part of the supernatant was saved as control. Microvesicle and exosome pellets were washed twice in PBS EVs free by ultracentrifugation (Optiman™ MAX-UP Ultracentrifuge) at their respective speeds for 40 minutes and resuspended in the final volume (70 μL of PBS EVs free).

To check the success of the isolation we measured the protein amount using spectrophotometer NanoDrop™ 2000c (Thermo Fisher Scientific), finally, samples were stored at 4°C for no more than 7 days.

Characterization

ISEV recommends characterizing EVs by at least three techniques. For this study, NIH-3T3-derived EVs were characterized by four techniques: Electron microscopy, Dynamic light scattering, Flow cytometry and Western blotting.

Electron microscopy Negative Staining

EVs characterization is commonly achieved by negative staining, a technique normally performed in bacteria or virus, and imaged in a transmission electron microscope (JEOL- JEM 1011 equipped with a high resolution Gatan digital camera). Protocol consists of applying 3 μL of EVs (previously obtained by ultracentrifugations) on the TEM-grid 10 seconds and blotted for 3 seconds; after that, sample was immediately stained with 10 μL of 0.5% uranyl acetate for 10 seconds and blotted again. Grid was air-dried 5 minutes and placed into a grid box until its observation (minimum drying time before observation: overnight).

Dynamic Light Scattering

To define the electric charge of the EVs under study we utilized dynamic light scattering using Malvern Zetasizer Ultra MADLS ®. We used PBS EVs free as control buffer, a 1:100 dilution was prepared, and samples were placed into 12 mm o.d. square glass cell cuvettes (PCS1115). Three measurements of each population of extracellular vesicles were performed and averaged.

Flow cytometry

Flow cytometry was carried out to measure the concentration of isolated EVs population.

Following characterization protocol MASCQuant® Analyzer cytometer, was used to measure the number of EVs per sample. Before measurement, channels were set up to hyper log (hlog), triggered on SSC to 4 and secondary trigger was shut off. An unstained control PBS EVs free was measured to evaluate background noise. Autofluorescence was evaluated by the measurement of unstained EVs samples (EVs from NIH-3T3 cells). To measure the samples, we performed 1:10 dilution in PBS EVs free (Rotator et al., 2015).

Western blotting

ISEV recommends that EVs must be characterize by at least three positive protein markers including at least one: transmembrane/lipid-bound protein or cytosolic protein. In this technique were used three different biological samples for each EVs type. To detect EVs marker proteins in our EVs samples the technique used was western blotting (WB). We measured the protein content of exosomes and microvesicles and 140 μg of EVs protein were loaded in each well, NIH-3T3 mKATE lysis, NIH-3T3 lysis, buffer lysis, depleted medium and the supernatant saved as mentioned in isolation section above, were used as control. Samples were separated by size in a 12% polyacrylamide gel (Flotillin-1 and Syntenin-1 antibodies) and in 15% (CD81 antibody) for 10 minutes at 100 V and then 90 minutes at 180 V with SDS-PAGE. Polyvinylidene difluoride (PVDF) membranes were used

for protein transfer. Membranes were activated 10 minutes in methanol. Transfer conditions were 90 minutes at 300 mA. After the transfer process membranes were blocked with 5% BSA (Bovine Serum Albumin)– TBS for 1 hour at room temperature in agitation. Then, membranes were incubated with primary antibodies (Flotillin- 1, Syntenin- 1 or CD81) overnight at 4°C in agitation. Three washes with TBST 10 minutes each were done, and then secondary fluorescence antibody against the specie of the primary antibody were incubated for 1h under dark conditions at room temperature in agitation. Finally, three TBST washes were done, and the membranes were visualized by Odyssey CLx Near-Infrared Fluorescence Imaging System. Images were analyzed using Image J software.

To confirm success transfer, gels were stained with Coomassie Blue Stain and membranes with Ponceau S Staining solution on agitation for 10 minutes and images were taken after TBST washes (**Figure** 10).

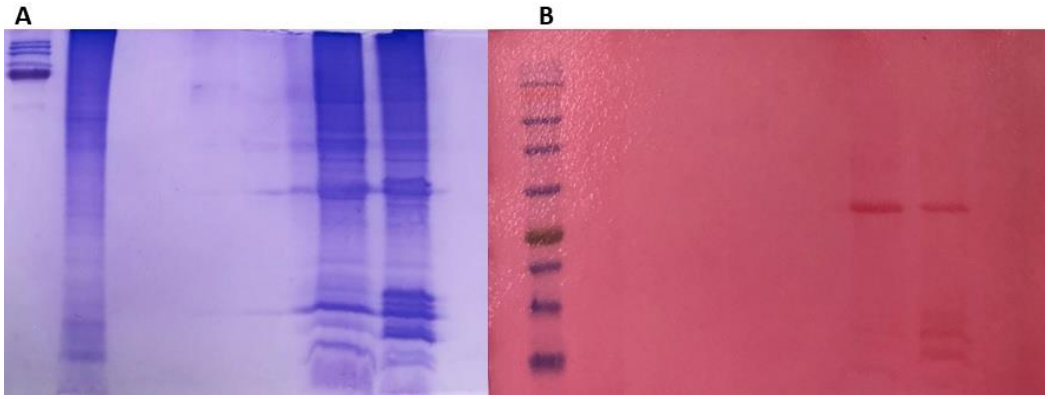

Figure 10. Unspecific protein detection to confirm a successful electrophoresis and transfer a) gel stained with blue coomasie; and a successful protein transfer to the membrane: b) membrane stained with red poceau. **Source:** author

cTPRAu-390 encapsulation into EVs

Isolated microvesicles (140 µg) and exosomes (80 µg) were mixed in a final concentration 25 µM of cTPRAu-390 and were incubated at room temperature in agitation for 15 minutes. Then, to increase the permeability of the plasma membrane of the extracellular vesicles and allow the nanocluster to enter into them, an electroporation technique was used. Samples were placed into electroporation cuvettes and electroporated using BIO-RAD Gene Pulser II Electroporator and Capacitance Extender Plus. Electroporation conditions were 400 V 125 µF two pulses (**Figure** 11). For subsequent microscopy visualization, the samples were stained with 3 µL of BODIPY™ TMR-X NHS Ester (Succinimidyl Ester) (Thermo Fisher Scientific) (fluorescent dye) that binds lipids unspecifically; and incubated in agitation for 15 minutes. In addition, to eliminate excess of dye and non- encapsulated cTPRAu-390, PBS EVs free washes were done by ultracentrifugation (at 10,000 × g microvesicles & 100,000 × g exosomes) for 40 minutes at 4°C. Finally, the pellet was resuspended in PBS EVs free. To *in vivo* study, BODIPY was not used to stained encapsulated cTPRAu-390 into EVs because its wavelength is not appropriate to be used in the Spectrum *In vivo* Imaging System (IVIS). Instead, DiR fluorescent dye was used (5 µL).

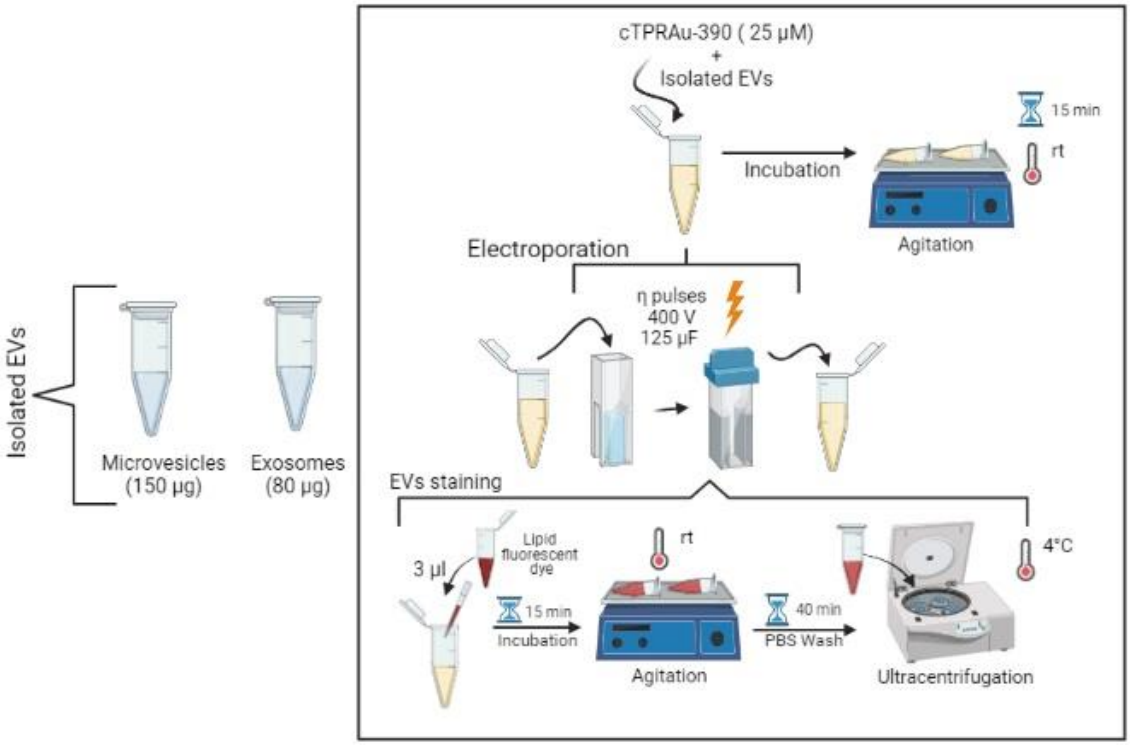

Figure 11. Scheme of the encapsulation of cTPRAu-390 into EVs by electroporation. Created with BioRender.com

Flow cytometry analysis to detect the encapsulation of the therapy into EVs

MASCQuant® Analyzer cytometer was used to analyze samples as described in Cytometry section with addition and set up of cTPRAu-390 and BODIPY fluorescence channels. Set aside control samples as described in encapsulation section were analyzed.

Different treatments for analyzing profibrotic gene expression in NIH-3T3 cells.

80,000 NIH-3T3 cells were seeded into T12 dishes with 3 mL medium. After 24 h with a 75% of cell confluence, cells were washed with PBS for treatments to be applied. 1 ng/mL TGF β and medium up to 1 mL were placed in each well. The first column was used as a control and no treatment was applied. 150 µg (protein amount) of microvesicles non encapsulated were applied into the second column and in the third one was added cTPRAu-390 encapsulated into (150 µg protein amount) microvesicles (**Figure** 12). In addition, the dish with treatments was incubated for 24 h or 36 h, after this time the medium was discarded, and the plate was stored at -80°C. The same process was performed for exosomes with the difference in the concentration of protein used, which was 80 µg (protein amount) for non and encapsulated exosomes.

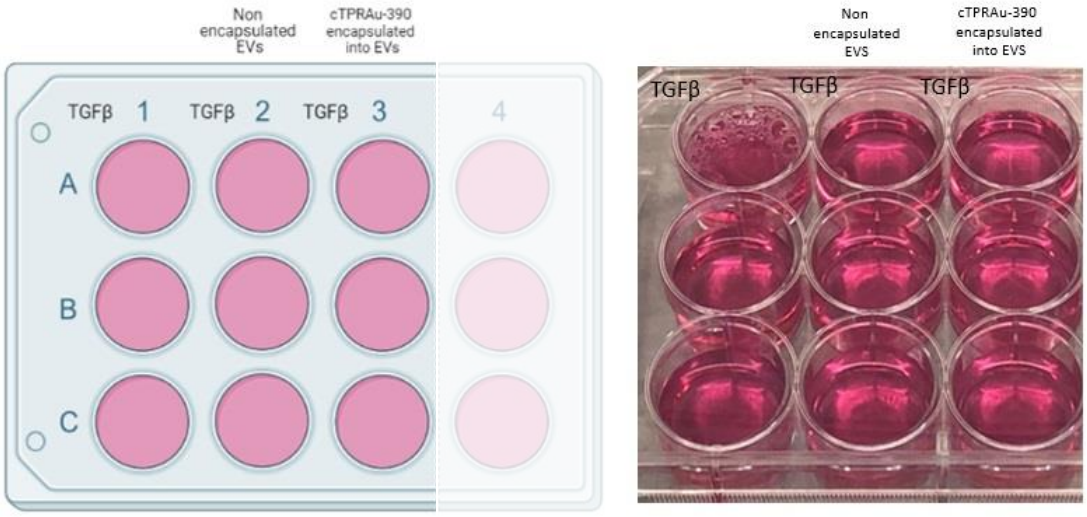

Figure 12. Scheme of different treatments. NIH-3T3 cells cultured on T12 dishes with the different treatments applied to each one of the wells: in every well was added 1ng/mL of TGF β; second column, 150 μg microvesicles or 80 μg exosomes & third column, cTPRAu-390 encapsulated into EVs. Created with BioRender.com

Study of gene expression of the genes of interest

RNA isolation

Once the cells described in the above section were frozen, we defrost cells and proceeded to RNA isolation, following NZYol (nzytech, MB18501, 100 mL) protocol as follows.

In the first step, cells were lysed by applying NZYol (1 mL/5×10^6 cells) and incubated for 5 minutes at room temperature.

The phases were separated by adding chloroform, shaken briefly, and incubated at room temperature for 3 minutes. Samples were centrifuged (Centrifuge 5810R, Eppendorf) at 12,000 × g for 15 minutes at 4°C, then aqueous phase that contains RNA (**Figure** 13) was carefully transferred into new tubes.

RNA was precipitated with cold isopropanol, incubated for 10 minutes at room temperature, and centrifuged for 10 minutes at 12,000 × g at 4°C. Then washed with cold 75% ethanol (1 mL of ethanol/1 mL NZYol), centrifuged at conditions mentioned above, the supernatant was discarded and well air dried before resuspended in RNase- free water. Samples were quantified by absorbance reading in the spectrophotometer (NanoDrop™ 2000c, Thermo Fisher Scientific).

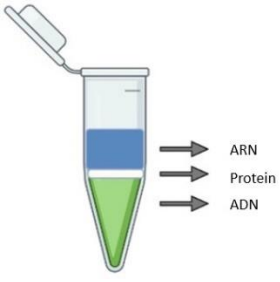

Figure 13. Separation of the different phases in RNA isolation, at the bottom DNA, at the middle protein and at the top RNA. Created with BioRender.com

Reverse Transcription

After obtaining the purified RNA, the cDNA was obtained using High-Capacity cDNA Reverse Transcription (RT) Kit, 1000 reactions (Thermo Fisher Scientific PN 4368813). We prepared 2× RT master mix (**Table** 1). 0.1 µg of ARN was used, water up to 10 µL and mixed with 10 µL of master mix. Thermal cycler conditions are illustrated in **Table** 2.

Table 1. 2× RT Master mix components to perform reverse transcription reaction to obtain cDNA from RNA. (Thermo Fisher Scientific PN 4368813)

Component	Volume/ Reaction (µL)
10× RT Buffer	2.0
25× RT dNTP Mix (100mM)	0.8
10× RT Random Primers	2.0
MultiScribe ™ Reverse Transcriptase	1.0
Nuclease-free H_2O	4.2
Total per Reaction	10.0

Table 2. Thermal cycler conditions for the reverse transcription reaction to obtain cDNA from RNA (Thermo Fisher Scientific PN 4368813)

Temperature °C	Time
25°C	10 min
37°C	2 h
85°C	5 min
12°C	∞

Real time PCR (qPCR)

To analyze genes expression of Col I, Col III and FN, we performed qPCRs in which the results are expressed as relative expression comparing to control sample expression in arbitrary units. We applied deltha-deltha Ct method ($2^{-\Delta\Delta ct}$): ΔΔCt= ΔCt (gene of interest) – ΔCt (housekeeping gen). We analyzed three conditions: first one corresponds to the control NIH-3T3 cells without treatments, the second one corresponds to EVs treatment and the third to cTPRAu-390 (25 µM) encapsulated into microvesicles. The same conditions were analyzed with exosomes.

Once we had cDNA, we proceeded to prepared master mix. PowerUp™ SYBR™ Green Master Mix was used in real time PCR for measurement of the expression of genes of interest (Col I, Col III and FN). Mouse ribosomal protein S14 was used as housekeeping gen because its basal expression level will always be expressed and will be used to relativize with the genes of interest. 1uL of 1:10 dilution of the cDNA was used as template. **Table** 3 illustrates thermal cycler conditions and in **Table** 4 primers used in qPCR.

Table 3. Thermal cycler conditions to be used in qPCR (Thermo Fisher Scientific Baltics UAB).

Step	Temperature	Duration	Cycles
UDG activation	50°C	2 minutes	Hold
Dual-Lock DNA polymerase	95°C	2 minutes	Hold
Denature	95°C	15 seconds	40 minutes
Anneal	60°C	15 seconds	
Extend	72°C	1 minute	

Table 4. Primers used for qPCR.

Gen		Sequence
Col1A1	F	TGG GGC AAG ACA GTC ATC GAA TA
Col1A1	R	GGG TGG AGG GAG TTT ACA CG
Col3A1	F	ACC CCA TGA TGT GTT TTG TGG CA
Col3A1	R	CAG GTC CTC GGA AGC CAC TA
Fibronectine	F	CAC CCA CAT GGC AGC TCA CA
Fibronectine	R	ATG GGA ACC CTG AAG CCA GC
S14	F	AGT GAC TGG TGG GAT GAA GG
S14	R	CTT GGT CCT GTT TCC TCC TG

EVs internalization assay

Fluorescence microscopy assays to visualize the internalization of EVs into cells

Nikon fluorescence ECLIPSE Ti2 inverted microscope was used for the visualization of the internalization of EVs. The settings of different channels are illustrated in **Table** 5, mCherry corresponds to EVs, GFP to BODIPY fluorescent dye and DAPI to cTPRAu-390 encapsulated into EVs. 1 x 10^5 NIH-3T3 cells were cultured on μ-Dish 35 mm, high microscopy dish which has an ibidi polymer coverslip bottom that has a highest optical quality allowing the laser to detect our sample, after 24 hours the medium was changed to Leibovitz for microscopy. First the untreated cells were recorded, then EVs in the presence of TGF β were added to the cell culture and a 5-minute video was performed. Internalization was visualized for both encapsulated and non-encapsulated EVs.

After each video, cells were fixed with formaldehyde for 20 minutes in agitation at room temperature, then dishes were washed with PBS EVs free and stored at 4°C.

Table 5. Channel's settings to be used in the fluorescence microscope.

	Excitation/ Emission	Channel	Exposure time	Leds	Intensity	Excitation filter	Emission filter
mKATE	588/633 nm	mCherry	50 ms	575 nm	10%	578/21 nm	641/75 nm
BODIPY	544/570 nm	GFP	100 ms	470 nm	90%	472/30 nm	520/35 nm
cTPRAu-390	374/440 nm	DAPI	100 ms	395 nm	10%	377/50 nm	447/60 nm

Confocal microscopy assays to detect internalized EVs

Fixed cells from dishes above mentioned were used to detect EVs internalization. To confirm the internalization of the EVs into the cells, the microscope Leica's confocal Sp5, the oil objective 63 with a 1.4 mm of opening and 2.5 zoom, were used. Seven z were taken, the step size as 1.13 µm. Channels used for the visualization were three: the first corresponds to EVs, the second to the fluorescent dye used and the third one to the nanocluster. Technical conditions are illustrated in **Table** 6.

Table 6. Technical specifications and channels set up for confocal microscope.

	Excitation/ Emission	Channels	Leds	Intensity	Excitation filter	Emission filter
mKATE	588/633 nm	mKATE	594	49%	610 nm	660 nm
BODIPY	544/570 nm	GFP	543	40% of 14%	550 nm	610 nm
cTPRAU	374/440 nm	DAPI	405	27%	415 nm	415 nm

Fibrotic mice generation

To induce cardiac fibrosis subcutaneous implantation of osmotic minipumps A mid-scapular incision was made, and a subcutaneous pocket was created for the micro-osmotic pump (0.25 µl per hour, 14 days, alzet) to be inserted. The pump was previously filled with an aqueous solution of angiotensin II (0.70 mg). The wound was closed with a suture. Mice were monitored daily for any discomfort, and they were euthanized 2 weeks after surgery (**Figure** 14).

In vivo imaging system experiments to visualized EVs distribution in different organs in a fibrotic mouse

The Spectrum *In Vivo* Imaging System (IVIS) was used to perform these set of experiments in which a sequence of images of different wavelengths are separated to remove the autofluorescence of the targets and reveal real fluorescence, this process is called Spectral unmixing. Three adult (16–20 weeks old) C57BL6 wild type (WT) mice were used for this process. The first mouse was designated for cTPRAu-390 encapsulated into microvesicles, the second for encapsulated cTPRAu-390 into exosomes and the last one as control. Live animals' studies were approved by the University of

Cantabria Institutional Laboratory Animal Care and Use Committee in compliance with the Guide for the Care and Use of Laboratory Animals (ILAR, 1985) and were conducted in accordance with the "European Directive for the Protection of Vertebrate Animals Used for Experimental and Other Scientific Purposes" (European Communities Council Directive 86/606/EEC).

After one week, cTPRAu-390 encapsulated into 240,000 exosomes and into 1,600,000 microvesicles was injected intraperitoneally (I.P.). *In vivo* fluorescence image was performed using IVIS to see the distribution of the therapy during the time (**Figure** 14). *In vivo* photos were taken at times: 0, 24 h and 6 days. Mice were euthanized and *ex vivo* photos were taken.

Animal handling was performed by accredited researcher and supervisor Jorge Ruiz.

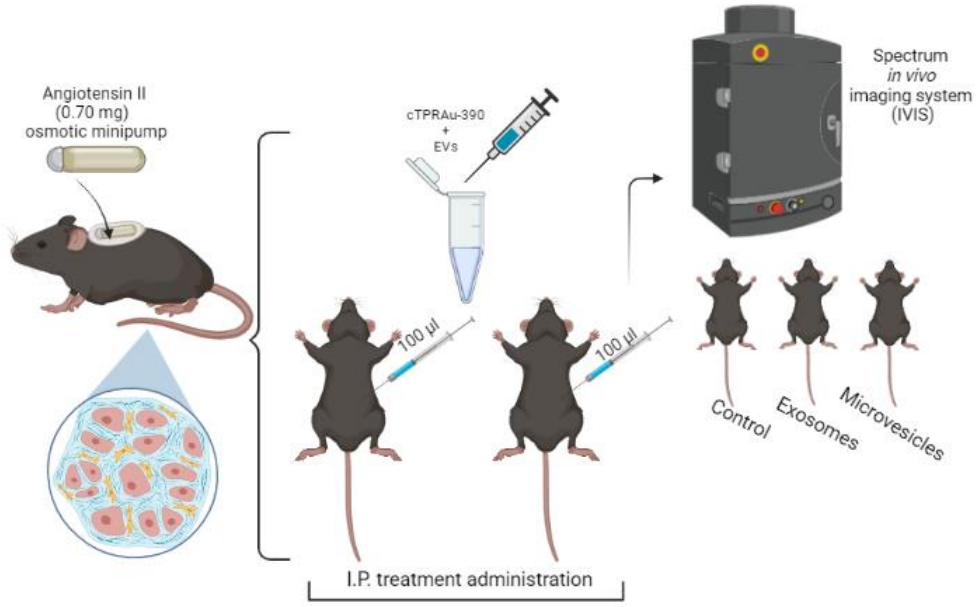

Figure 14. Scheme of the application of osmotic minipumps filled with Angiotensin II (0.70 mg) to induce cardiac fibrosis in mice, the administer of the treatment and visualization in IVIS. Created by Biorender.com

4. Results

Protein concentration of NIH-3T3-derived EVs

We obtained for microvesicles a protein concentration between 2.548 - 21.623 mg/mL and for exosomes between 1.11- 22.600 mg/mL depending on the yield of the isolation.

EVs characterization

1. Diameter of EVs

We obtained microvesicles with diameters in a range of 41.55 nm to 158 nm by electron microscopy technique, which is in accordance to the describe diameters for this population of vesicles (**Figure**

15) (de Abreu et al., 2020; Lawson et al., 2016; Sluijter et al., 2014). Additional images of microvesicles diameters are visualized in **Appendix** 1.1.

In the case of the exosome samples, the range was from 31.40 nm to 107.49 nm which also is in accordance with previously described exosomes diameters (**Figure** 16) (de Abreu et al., 2020; Ha et al., 2016; Kalra et al., 2016; Lamichhane et al., 2015; Y. Zhang et al., 2019). Additional images of exosomes diameters are visualized in **Appendix** 1.2.

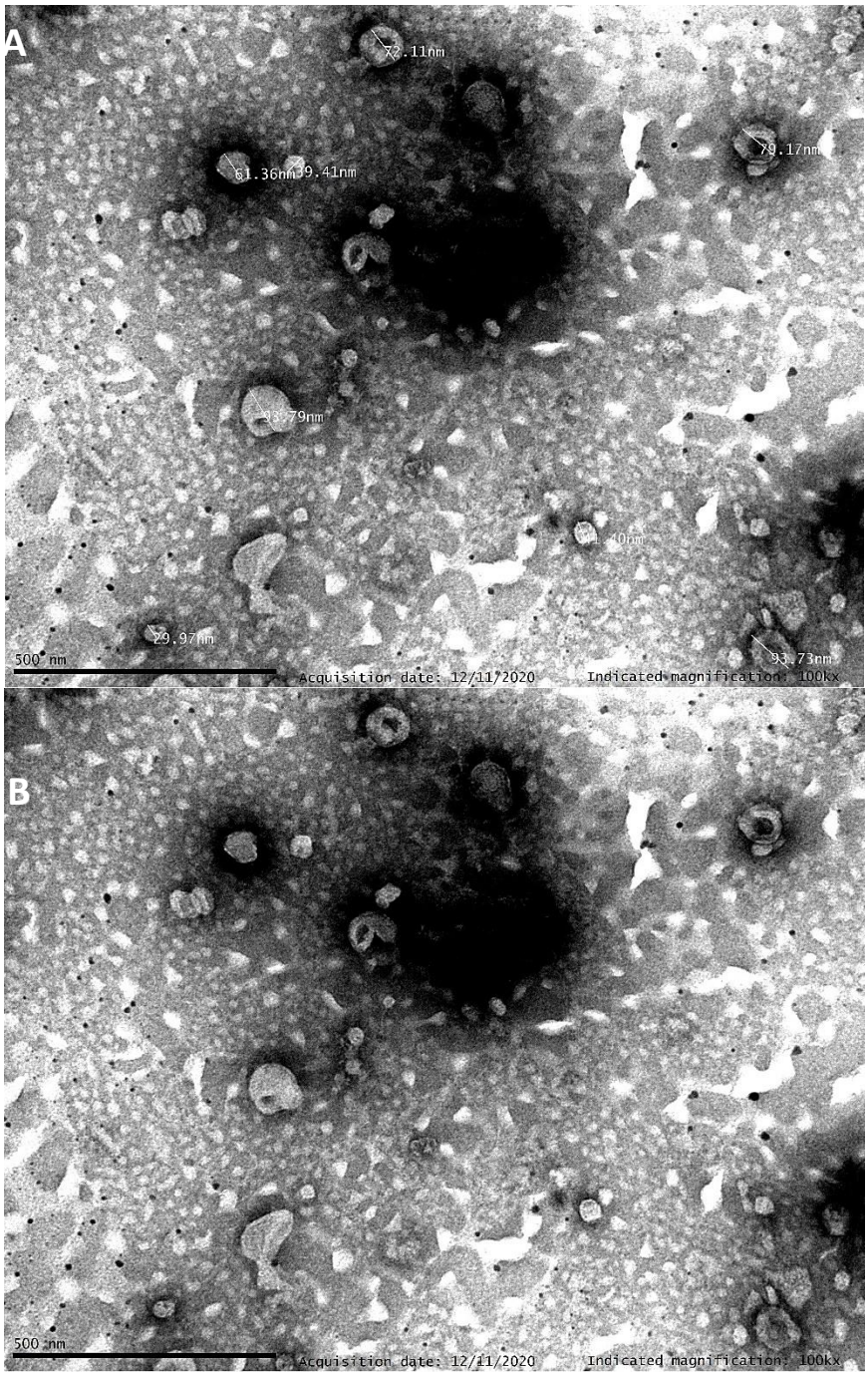

Figure 15. Microvesicles diameter size visualized by electron microscopy. a) microvesicles with sizes described, b) better visualization of microvesicles shape.

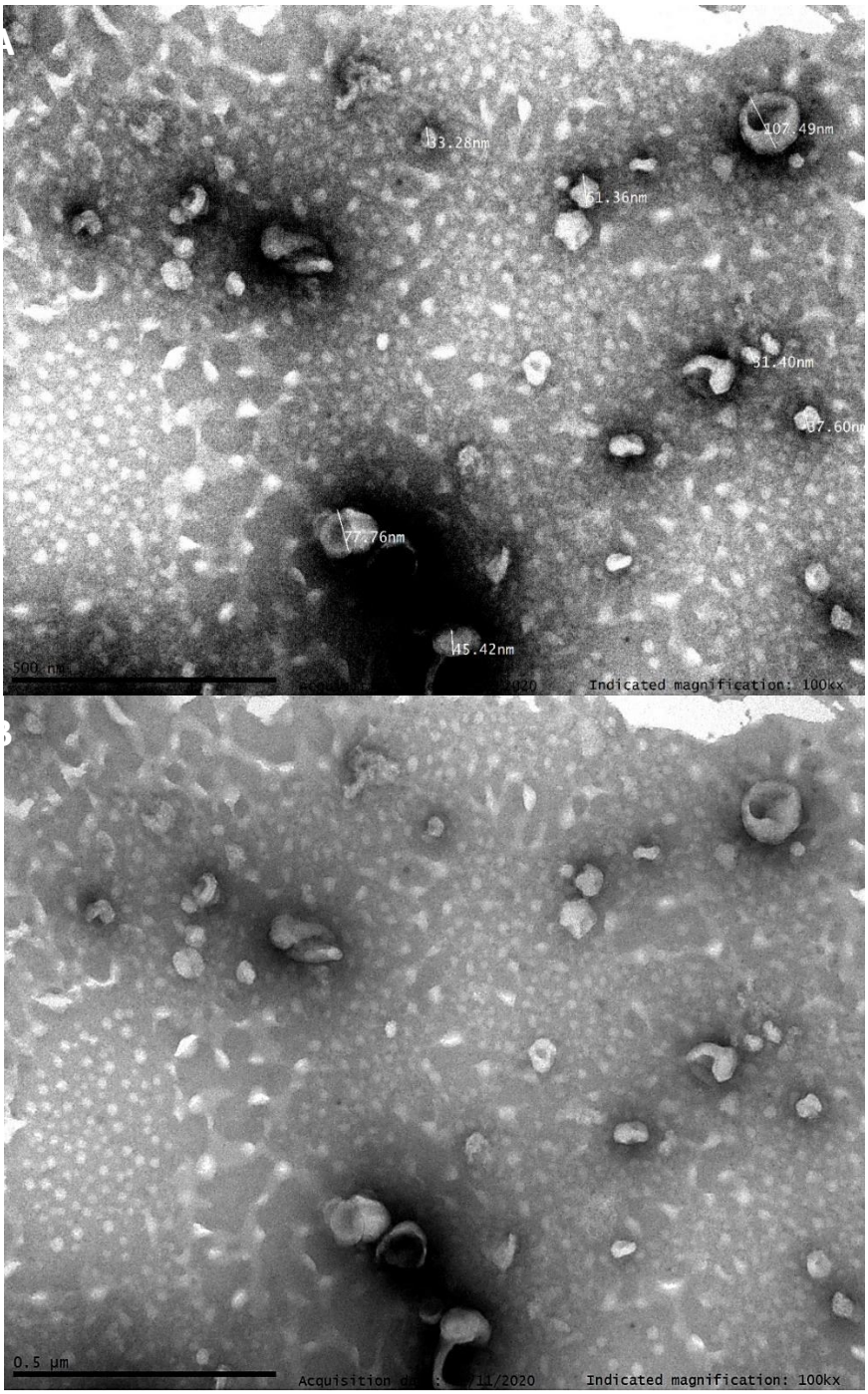

Figure 16. Exosomes diameter size visualized by electron microscopy. a) exosomes with sizes described, b) better visualization of exosomes shape.

2. Charge measurement of EVs

We obtained a neutral charge for microvesicles with an average – (0.047±0.01) mV with n_1= -0.05155, n_2=0.05585 and n_3=0.03416 (**Figure** 17). However, a negative charge was obtained for exosomes with an average of – (17.07±0.09) mV with n_1= -17.18; n_2=-17.04 and n_3=-16,99 (**Figure** 18).

n_1

Statistics Table

Name	Mean	Standard Deviation	RSD	Minimum	Maximum
Zeta Potential (mV)	-0,05155	-	-	-0,05155	-0,05155

n_2

Statistics Table

Name	Mean	Standard Deviation	RSD	Minimum	Maximum
Zeta Potential (mV)	0,05585	-	-	0,05585	0,05585

n_3

Statistics Table

Name	Mean	Standard Deviation	RSD	Minimum	Maximum
Zeta Potential (mV)	0,03416	-	-	0,03416	0,03416

Figure 17. Data obtained from Zsizer DLS of three different measurements of microvesicles.

n_1

Statistics Table

Name	Mean	Standard Deviation	RSD	Minimum	Maximum
Zeta Potential (mV)	-17,18	-	-	-17,18	-17,18

n_2

Statistics Table

Name	Mean	Standard Deviation	RSD	Minimum	Maximum
Zeta Potential (mV)	-17,04	-	-	-17,04	-17,04

n_3

Statistics Table

Name	Mean	Standard Deviation	RSD	Minimum	Maximum
Zeta Potential (mV)	-16,99	-	-	-16,99	-16,99

Figure 18. Data obtained from Zsizer DLS of three different measurements of exosomes.

3. Analysis of the number of EVs per sample

The first row of the tables in **Figure** 19 and **Figure** 20 corresponds to the total counts detected and the second row to the counts present in the region defined for EVs.

Image of control PBS (EVs free) buffer used for analysis is attached to **Appendix** 2.1. In **Figure** 19, on the left side, inside the region mark we obtained a 203,000 microvesicles/mL (counts/mL). This sample was 1:10 diluted, thus the stock solution of microvesicles was of 2,030,000 microvesicles/mL (counts/mL).

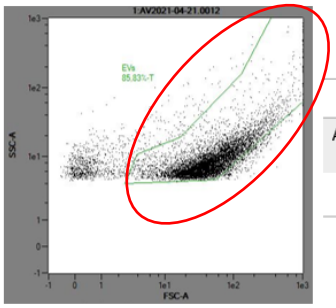

Path	SID	%-T	%-#	Count	Count/mL
AV2021-04-21.00012	Microvesicles	100.00	--	9443	2.36e5
EVs	Microvesicles	85.83	85.83	8105	2.03e5

Figure 19. Measurement of microvesicles concentration by forward scatter versus side scatter of 1:10 sample dilution. Red mark encloses expected population shape in microvesicles by flow cytometry.

In **Figure** 20, on the left side, inside the region mark we obtained 11,300,000 exosomes/mL (counts/mL). As before, the sample was 1:10 diluted so we got 113,000,000 exosomes/mL (counts/mL).

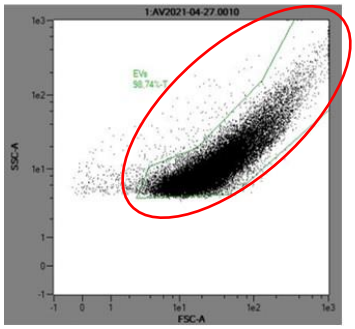

Path	SID	%-T	%-#	Count	Count/mL
AV2021-04-27.0001	Exosomes	100.00	--	45986	1.15e6
EVs	Exosomes	98.74	98.74	45408	1.13e6

Figure 20. Measurement of exosomes concentration by forward scatter versus side scatter of 1:10 sample dilution. Red mark encloses expected population shape in exosomes by flow cytometry.

4. Detection of EVs markers

We checked three biomarkers for EVs such as Flotillin-1 whose expected band size was 47kDa, Syntenin-1 whose expected band size was 33 kDa and CD81 whose expected band size was 25kDa.

As is illustrated in **Figure** 21, gel stained with Coomassie blue confirms a correct electrophoresis of the gel and its transfer to the membrane. We observed Flotillin-1 at the described weight in both fraction (Microvesicles and exosomes) in three independent experiments. The relative quantification of the band intensities correspondent to Flotillin-1 offered not significant differences between Flotillin-1 protein expression of microvesicles and exosomes and showed us that Flotillin-1 is expressed in both type of EVs.

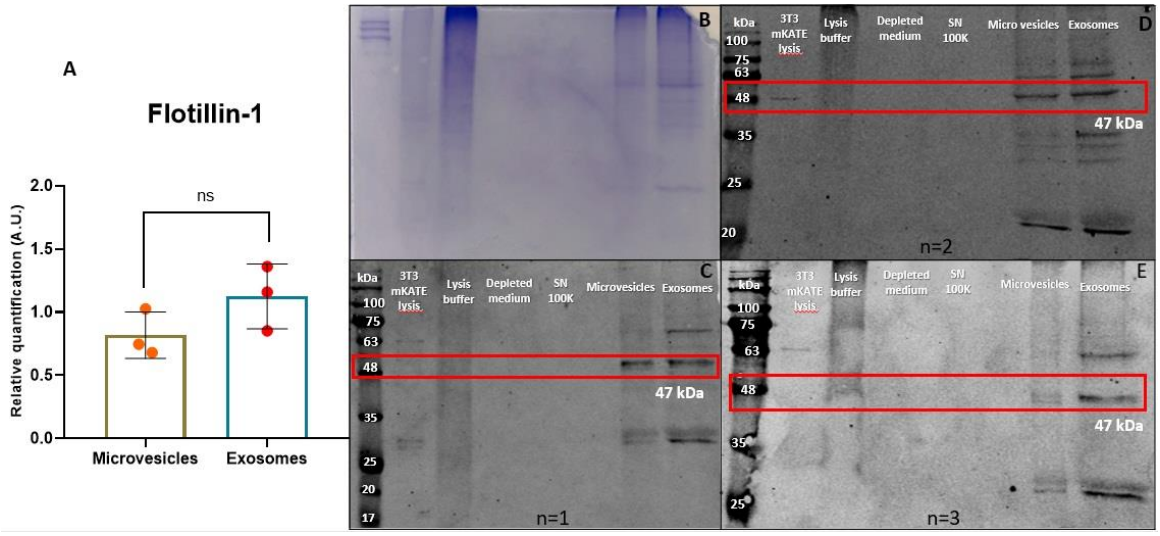

Figure 21. a) Quantification (Image J software) of Fotillin-1 protein expression in EVs showing non significance differences between microvesicles and exosomes, b) gel stained with Coomassie blue confirm the correct electrophoresis, c, d & e) Different membranes with expected Flotilin-1 molecular weight 47kDa.

Next biomarker to analyze was Syntenin-1. We observed Syntenin-1 at the described molecular weight in both fractions (Microvesicles and exosomes) in three independent experiments (**Figure** 22). Syntenin-1 was 33 kDa and we see that in microvesicles are more quantity of this biomarker. The relative quantification of the band intensities offered not significant differences between microvesicles and exosomes indicating that Syntnein-1 is expressed in both type of EVs. In **Figure**

22 is also shown gel stained with Coomasie blue, and membrane stained with red ponceau to confirm a correct electrophoresis of the gel and its transfer to the membrane.

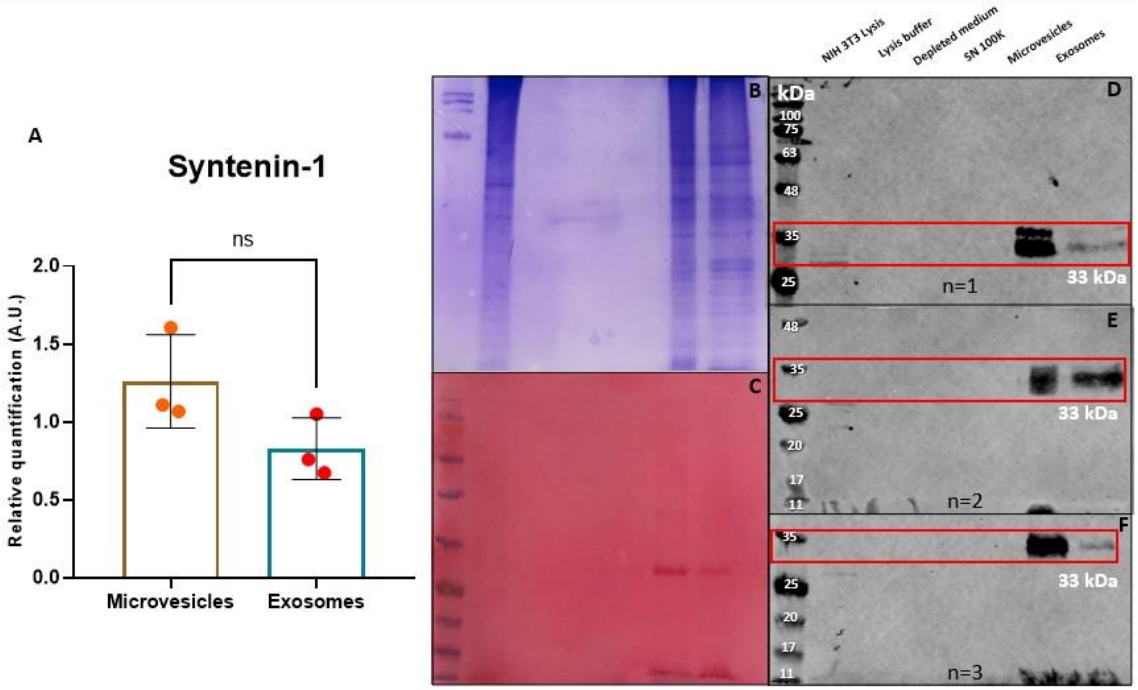

Figure 22. a) Quantification (Image J software) of Syntenin-1 in EVs detected by WB showing non significance between them; b & c) Gel stained with Coomasie blue and membrane stained with red ponceau confirm correct electrophoresis of the gel and its transfer to the membrane; d, e & f) Different membranes with expected Flotilin-1 molecular weight 33 kDa.

In **Figure** 23, gel stained with Coomasie blue, and membrane stained with red ponceau confirms a correct electrophoresis of the gel and its transfer to the membrane. We observed CD81 at the described weight in both fraction (Microvesicles and exosomes) in three independent experiments. CD81 was 25 kDa and we see that in microvesicles and exosomes are same quantity of this biomarker. The relative quantification of the band intensities correspondent to CD81 offered not significant differences between CD81 protein expression between microvesicles and exosomes and showed us that CD81 is expressed in both type of EVs.

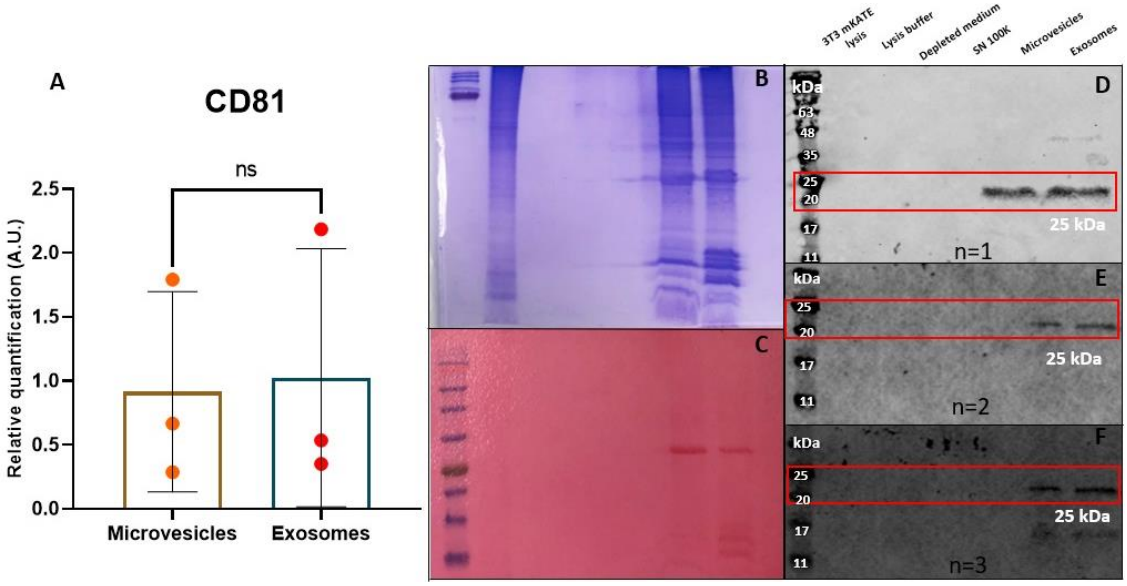

Figure 23. Quantification (Image J software) of CD81 in EVs showing non significance between them; b & c) Gel stained with Coomasie blue and membrane stained with red ponceau confirm correct electrophoresis of the gel and its transfer to the membrane; d, e & f) Different membranes with expected Flotilin-1 molecular weight 25 kDa.

Analysis of the encapsulation of cTPRAu-390 into EVs

Percentage of cTPRAu-390 encapsulated under different electroporation conditions is illustrated in **Table** 7. 0.25% and 13,39% of cTPRAu-390 was encapsulated into microvesicles and exosomes respectively and used for the experiment of gene expression at 24 h. 1.87% and 4.39% of cTPRAu-390 was encapsulated into microvesicles and exosomes for the experiment of gene expression at 36 h. For internalization experiment, was encapsulated 0.98% and 3.57% of cTPRAu-390 into microvesicles and exosomes, correspondingly. Finally, 1.87% it was encapsulated into microvesicles and 2.77% into exosomes and used for *in vivo* study. Images of PBS (EVs free) control, cTPRAu-390 control, non-encapsulated and encapsulated cTPRAu-390 into EVs, non-encapsulated and encapsulated cTPRAu-390 stained with BODIPY and DiR are supplemented in **Appendix** 2 section.

Table 7. cTPRAU-390 encapsulation percentage into EVs used in the different treatments.

	EVs	Counts/ml	Encapsulation %	Observations
In vitro 24 h	Microvesicles	1.95e6	0.25	2 pulses
	Exosomes	3.22e5	13.39	
In vitro 36 h	Microvesicles	2.21e6	1.87	2 pulses
	Exosomes	6.71e5	4.39	
Internalization	Microvesicles	5.67e6	0.98	5 pulses (damaged)
	Exosomes	3.82e5	3.57	3 pulses
In vivo study	Microvesicles	1.59e6	1.87	2 pulses
	Exosomes	2.36e5	2.77	

Genes expression analysis

Three independent experiments and triplicate for each experiment were performed in this analysis. As seen in **Figure** 24, after 24 hours of incubation of the treated cells there was not variation in Col I, Col III or FN gene expression under the following conditions: presence of TGF β, presence of TGF β and microvesicles and presence of TGF β and cTPRAu-390 encapsulated into microvesicles.

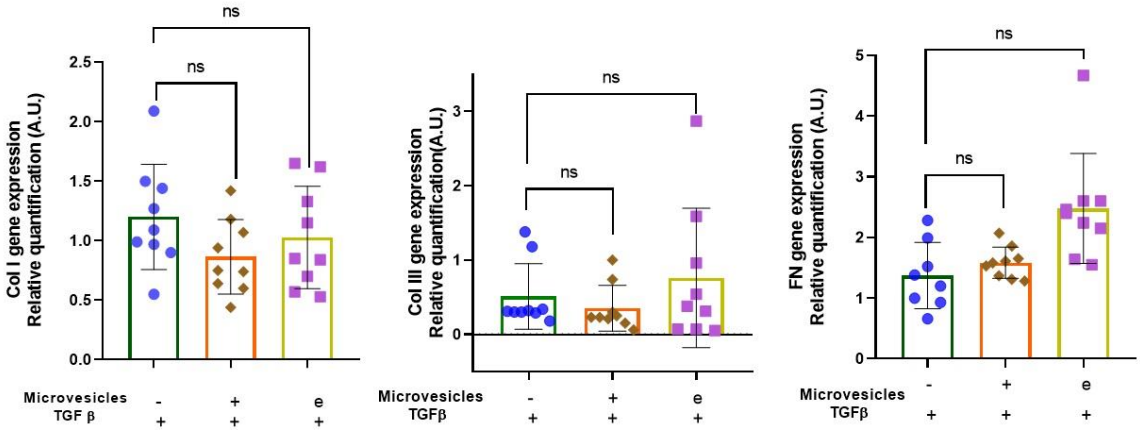

Figure 24. Lack of variation of Col I, Col III and Fibronectin gene expression after incubation with microvesicles or cTPRAu-390 encapsulated into microvesicles for 24 h Student T test. e refers to cTPRAu-390 encapsulated into microvesicles, - to Non microvesicles, + to Microvesicles, + to TGF β.

Same conditions used as in the above assays were used for experiment at 36 h for microvesicles and exosomes. Three independent experiments and triplicate for each experiment were performed in this analysis.

As is shown in **Figure** 25, there was not significant difference between treatment with microvesicles and control, being significant with the encapsulated therapy. We see that Col I, Col III and Fibronectin expression was significantly reduced in presence of cTPRAu-390 encapsulated into microvesicles.

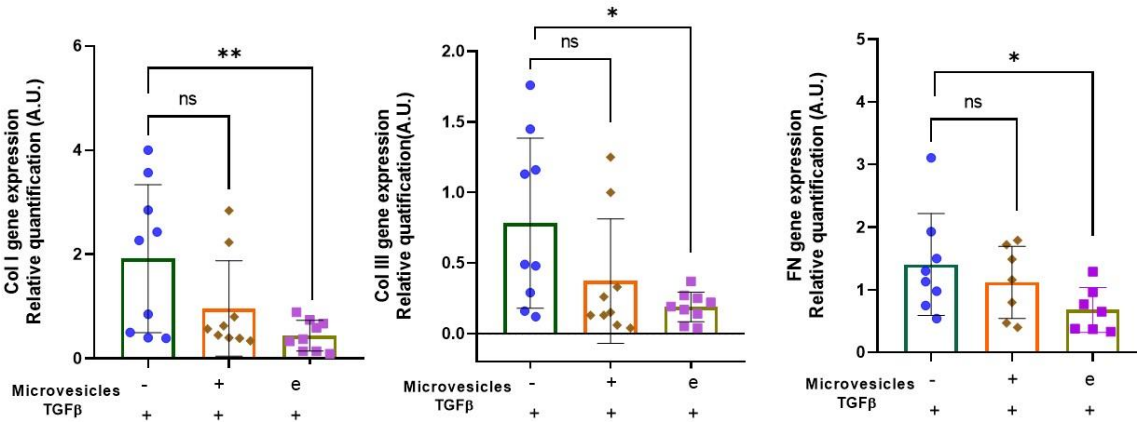

Figure 25. Decreased expression of Col I, Col III and Fibronectin gene expression after incubation with cTPRAu-390 encapsulated into microvesicles for 36 h. Student T test ** P< 0.005; *P <0.05. e cTPRAu-390 encapsulated into microvesicles, - Non Microvesicles; + Microvesicles, + TGF β.

In **Figure** 26, we observed a significant difference in Col I expression with unencapsulated exosomes treatment, being more significant with cTPRAu-390 encapsulated therapy. For Col III and FN genes, there is no significant difference in the column corresponding to the treatment of exosomes without encapsulation, being significant with the encapsulated therapy.

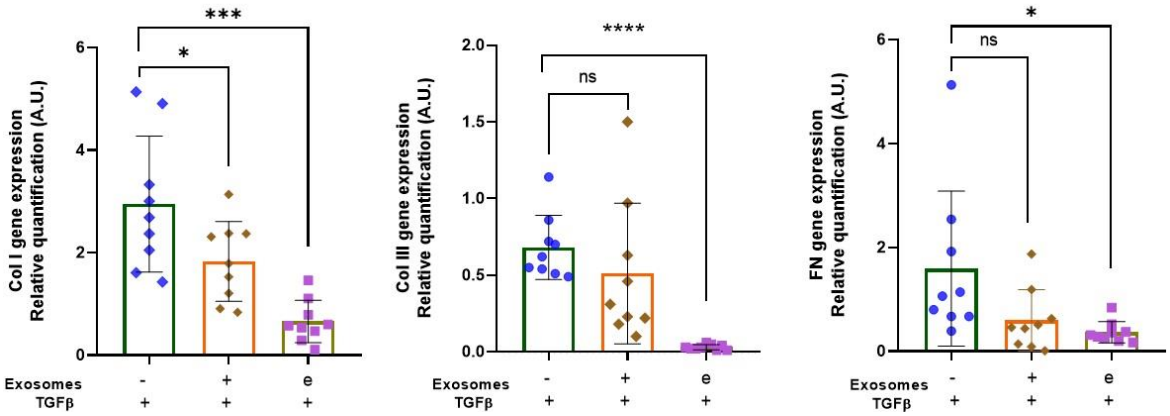

Figure 26. Higher decreased expression in Col I, Col III and Fibronectin in the presence of exosomes treatment at 36 h. Student T test *** P< 0.0005, ****P<0.0001, * P <0.,05; e cTPRAu-390 encapsulated into exosomes, - Non exosomes, + Exosomes, + TGF β.

Detection of EVs internalization

The following channels were used for the detection and visualization of EVs internalization: the merged channel shows the mix of the fluorescence of all channels, mKATE shows the fluorescence of the EVs in red, BODIPY fluorescence used to stain the EVs in green, cTPRAu-390 fluorescence in blue and the bright field to visualize NIH-3T3 cell shape. All channels are used for non-encapsulated and encapsulated EVs, except for cTPRAu-390, which is used only for encapsulated EVs.

Figure 27 (Image J Software) illustrates the frames of the timelapse video of the internalization of the non-encapsulated microvesicles into the cell visualized in different channels mentioned above. The pathway of the microvesicles can be visualized in **Figure** 27 A & B, then the adherence to the cell **Figure** 27 C and the internalization **Figure** 27 D. **Figures** 28 and 29 illustrate the internalization of the non-encapsulated microvesicles in the merged and mKATE channel. As mentioned in previous sections, since the microvesicles were damaged by electroporation and were not encapsulated, the timelapse of the encapsulated microvesicles was not performed.

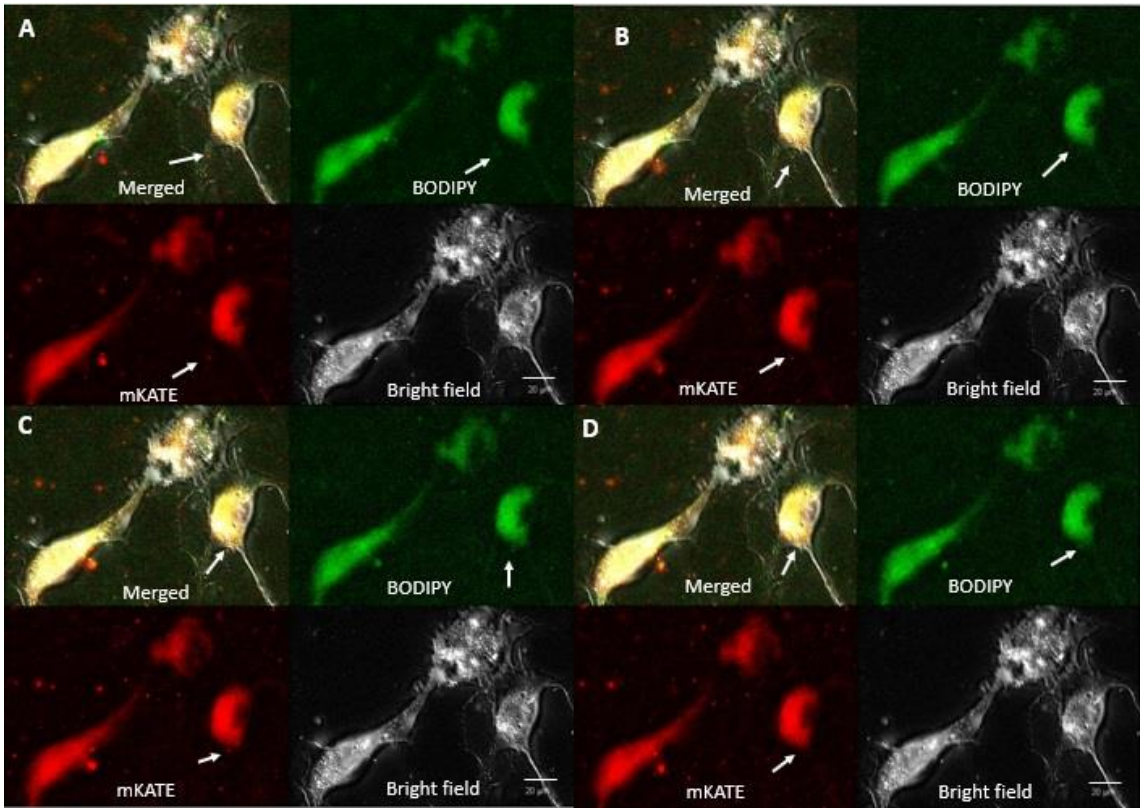

Figure 27. Frames obtained by the timelapse of microvesicles internalization into NIH-3T3 cells. a, b & c) microvesicles moving in direction to the plasma membrane, d) internalization into the cell (Image J software). **Source:** edited by the author.

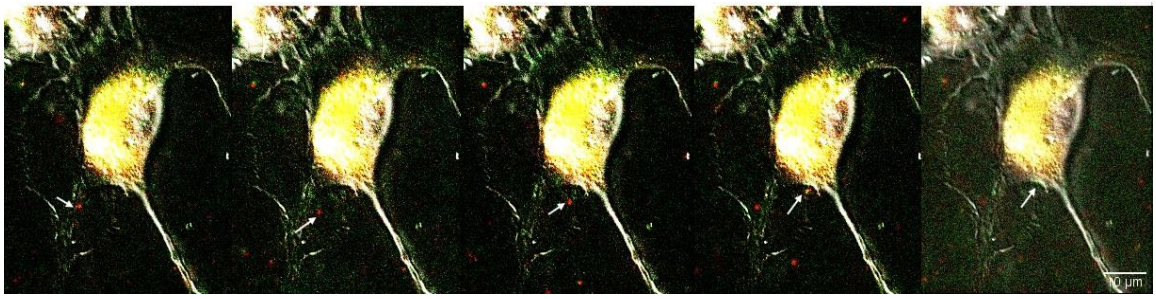

Figure 28. Frames of the internalization of microvesicles visualized by merged channel, microvesicles are represented as red-green spots (Image J software). **Source:** edited by the author.

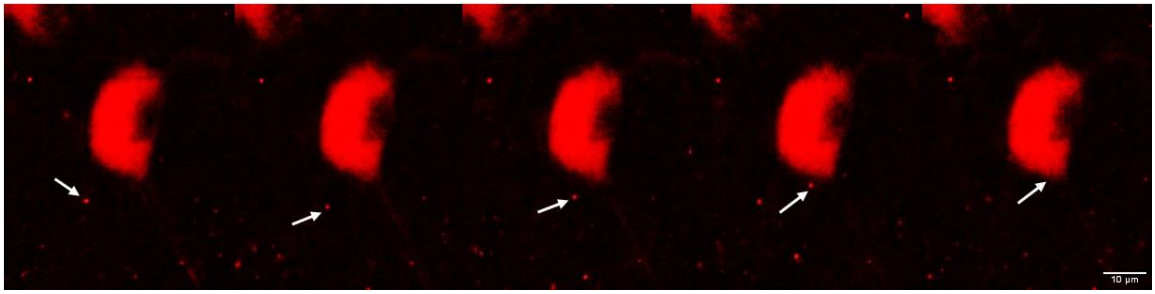

Figure 29. Frames of the internalization of non-encapsulated microvesicles visualized by mKATE channel, microvesicles are represented as red spots (Image J software). **Source:** edited by the author.

Figure 30 (Image J Software) illustrates the frames of the timelapse video of the internalization of the non-encapsulated exosomes into the cell in the different channels. The pathway of the exosomes

can be visualized in **Figure** 30 A, the adherence to the plasmatic membrane (**Figure** 30 B) and then the internalization **Figure** 30 C. **Figures** 31 and 32 illustrate closer the internalization of the non-encapsulated exosomes in the merged channel.

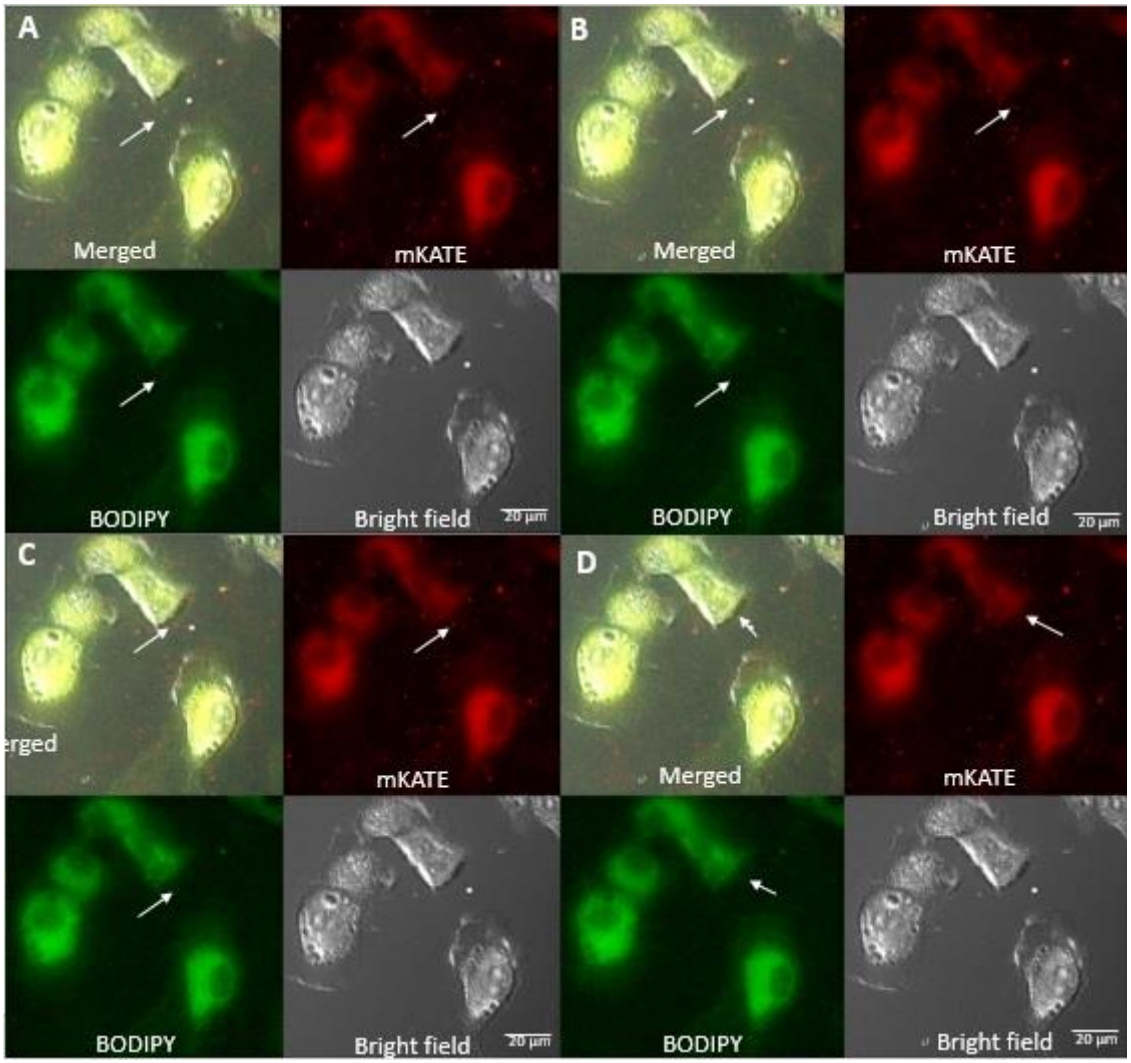

Figure 30. Frames obtained by the timelapse of exosomes internalization. a & b) exosomes moving to the plasmatic membrane, c) exosomes internalization into plasma membrane (Image J software). **Source:** edited by the author.

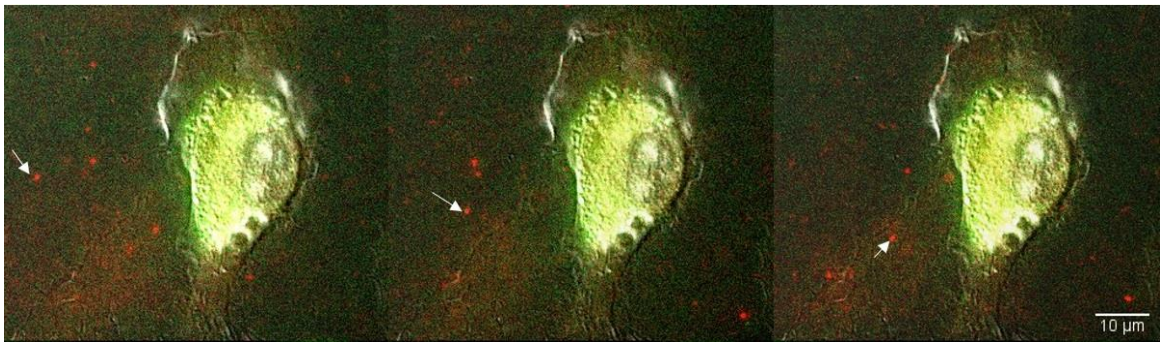

Figure 31. Frames of the internalization of exosomes visualized by merged channel, exosomes are represented as red-green spots (Image J software). **Source:** edited by the author.

Another event of non- encapsulated exosomes internalization is shown in **Figure** 32, the movement of exosomes into the cell can be visualized in **Figure** 32 A, B & C and then the internalization in **Figure** 32 D. In **Figure** 33 is visualized closer the internalization of the non-encapsulated exosomes by merged channel and in **Figure** 34 by mKATE channel.

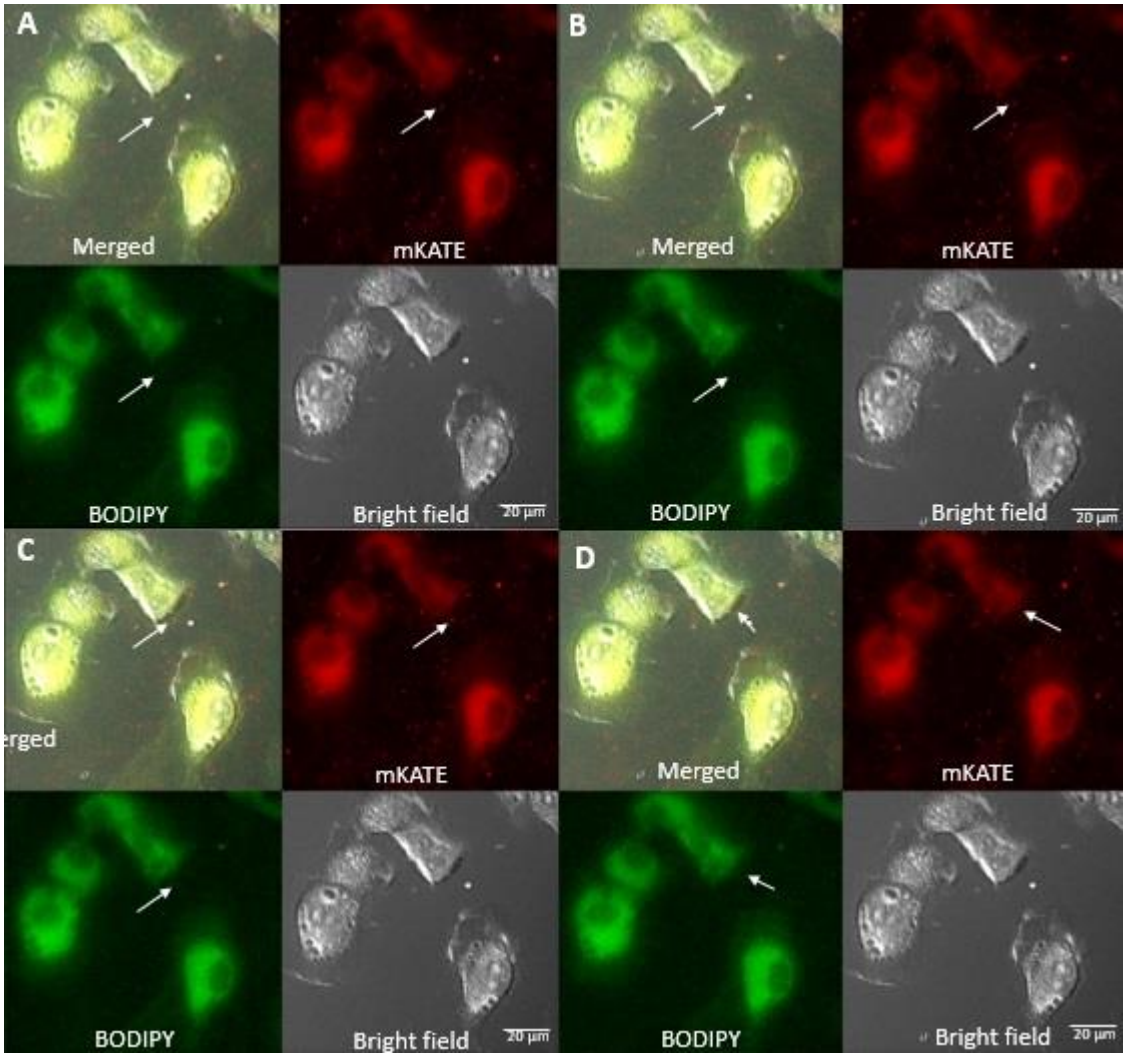

Figure 32. Frames obtained by the timelapse of exosomes internalization. a, b & c) exosomes moving to the plasmatic membrane, c) exosomes internalization into NIH-3T3 cell (Image J software). **Source:** edited by the author.

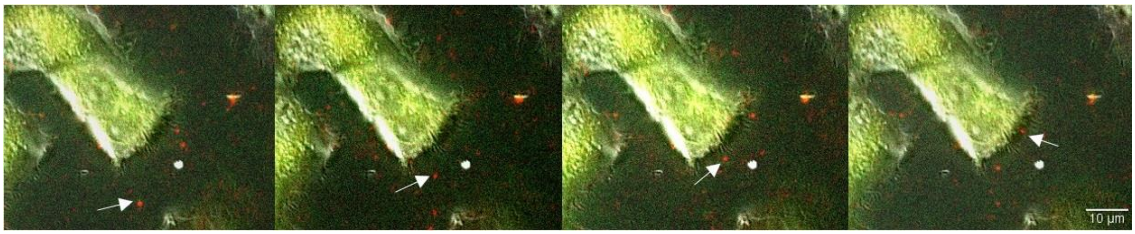

Figure 33. Frames of the internalization of exosomes visualized by merged channel, exosomes are represented as red-green spots (Image J software). **Source:** edited by the author.

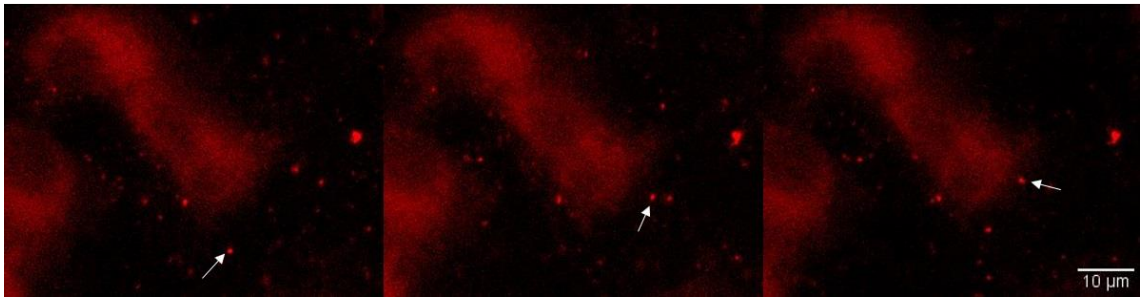

Figure 34. Closer visualization of the internalization of exosomes into NIH-3T3 cell shown in mKATE channel, exosomes are represented as red spots (Image J software). **Source:** edited by the author.

Figure 35 (Image J Software) illustrates the frames of the timelapse video of the internalization of cTPRAu-390 encapsulated into exosomes in the different channels. Exosomes are seen moving toward the plasma membrane as visualized in **Figure** 35 A & B, get attached to the cell **Figure** 35 C and then the internalization **Figure** 35 D. **Figure** 36 demonstrates the internalization of the cTPRAu-390 encapsulated into exosomes visualized by the merged channel.

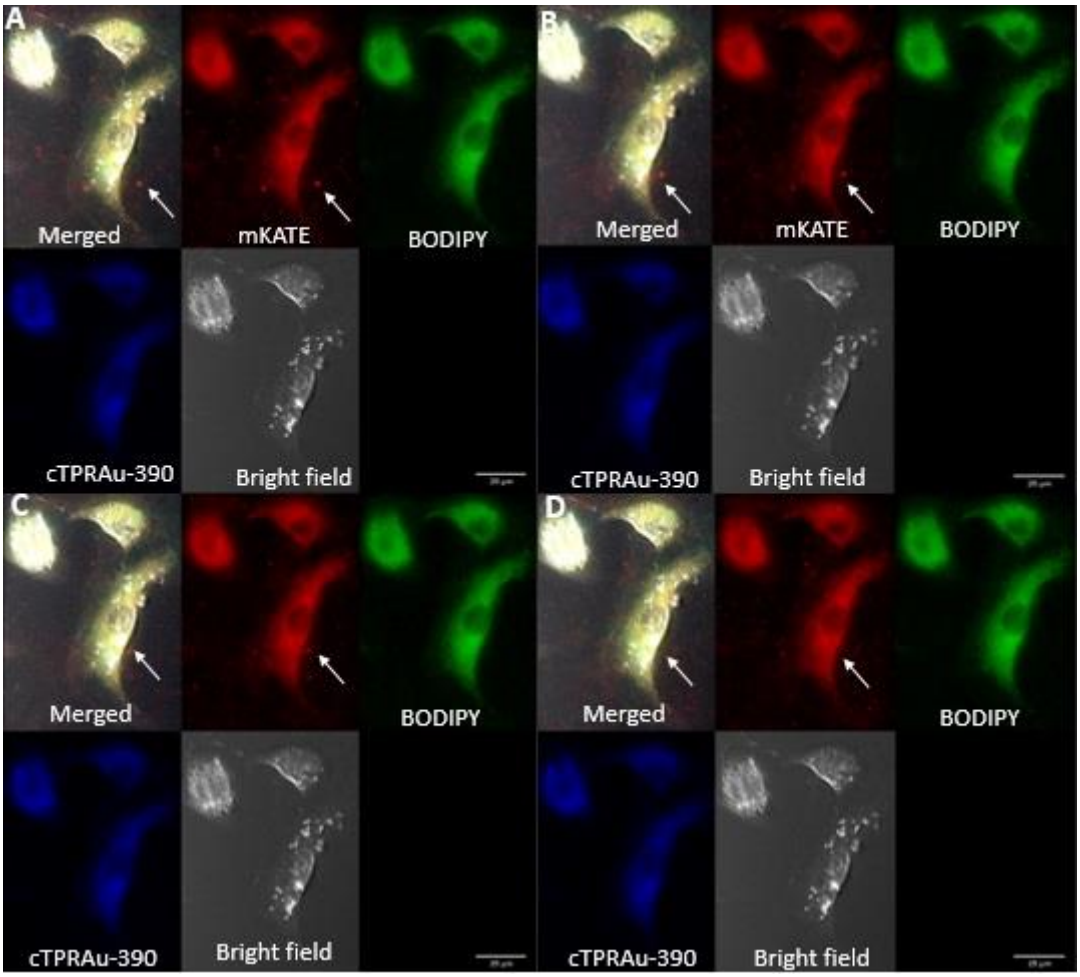

Figure 35. Frames obtained by the timelapse of cTPRAu-390 encapsulated into exosomes internalization. a, b & c) exosomes moving to the plasmatic membrane, d) exosomes internalization into NIH-3T3 cell (Image J software). **Source:** edited by the author.

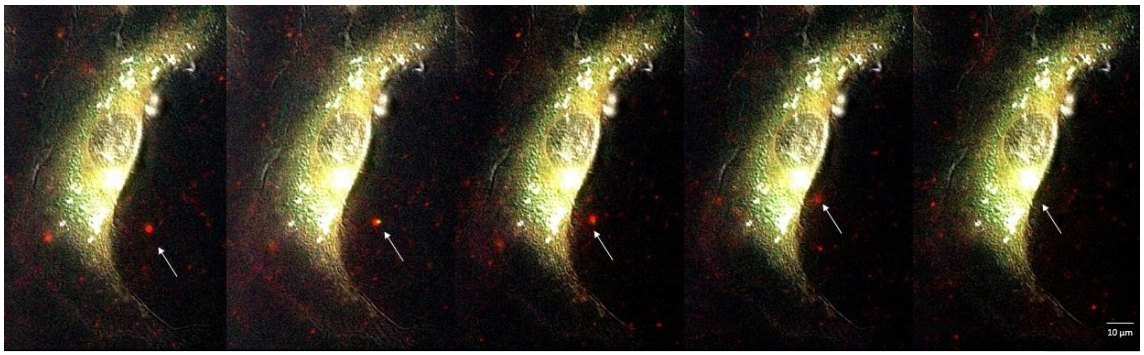

Figure 36. Closer illustration of cTPRAu-390 encapsulated into exosomes internalizing in the cell (Image J software) visualized in merged channel. **Source:** edited by the author.

The internalization of EVs in the cell was confirmed by confocal imaging in which the same channels were used. It is shown in **Figures** 37 and 38 the merged of different channels and it is demonstrated the internalization into the cell of the encapsulated nanocluster. **Figure** 37 corresponds to non-encapsulated microvesicles and **Figure** 38 to cTPRAu-390 encapsulated into exosomes.

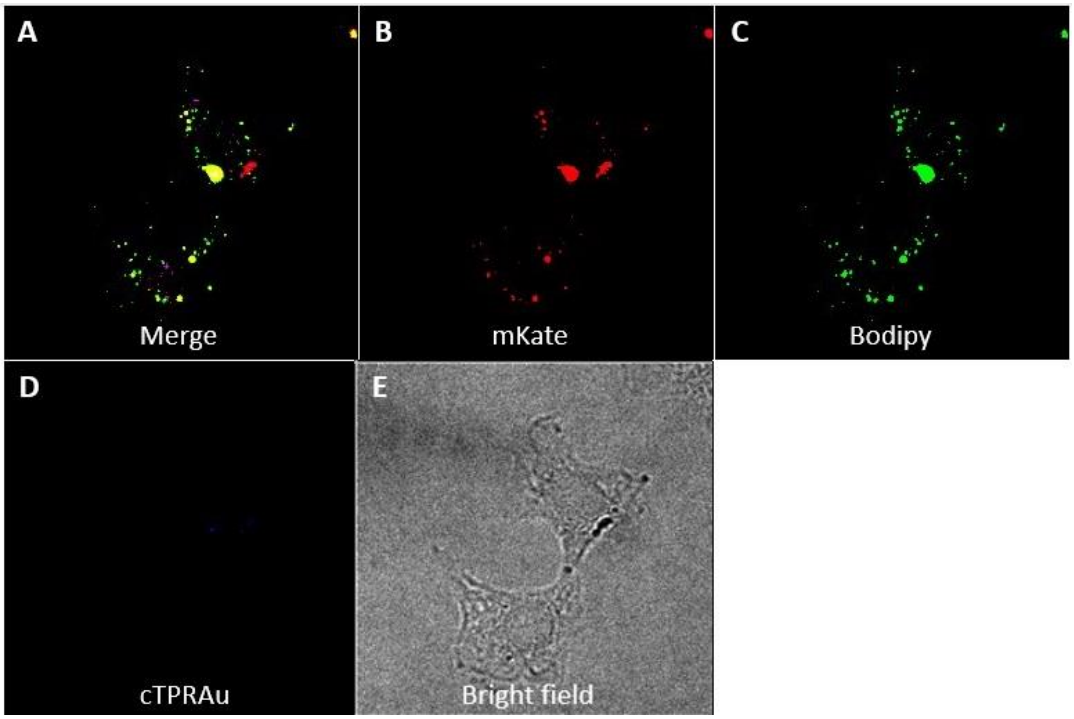

Figure 37. Non encapsulated cTPRAu-390 into microvesicles: a) Merge of different channels in which yellow color is the result of the mix of mKATE and Bodipy fluorescence, b) red fluorescence corresponds to microvesicles, c) green fluorescence by stained microvesicles, d) cTPRAu-390 blue fluorescence, as the microvesicles were not encapsulated, there was no presence of this fluorescence, d) bright field shows the cell (Image J software). **Source:** edited by the author.

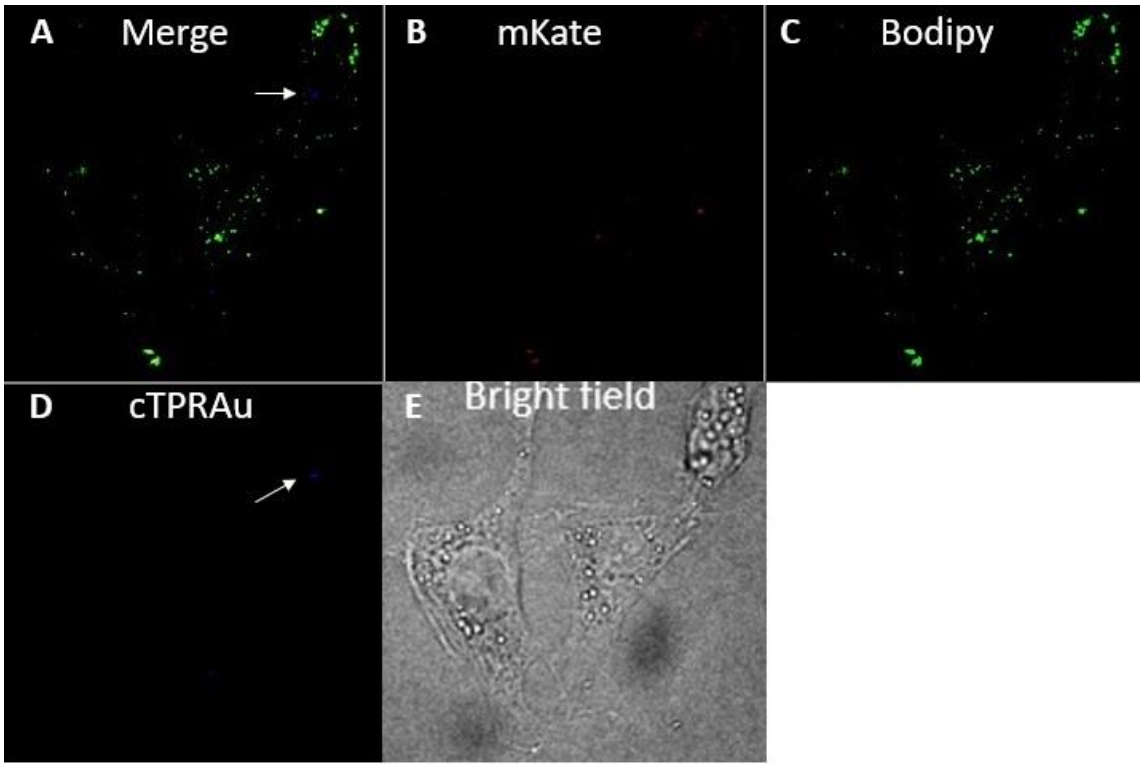

Figure 38. Confocal images showing exosomes and cTPRAu-390 detection: a) all channels combine b) red fluorescence of exosomes, c) green fluorescence by stained exosomes, d) cTPRAu-390 blue fluorescence, e) bright field to visualize NIH-3T3 cell shape (Image J software). **Source:** edited by the author.

EVs distribution in fibrotic mice through *in vivo* imaging and after EVs administration

The Spectral Unmixing *in vivo* at time 0 is illustrated in **Figure** 39. It is observed autofluorescence as green in control mouse, nor fluorescence in mouse with exosomes, whereas in mice with microvesicles a blue fluorescence is seen around administration area which corresponds to EVs fluorescence.

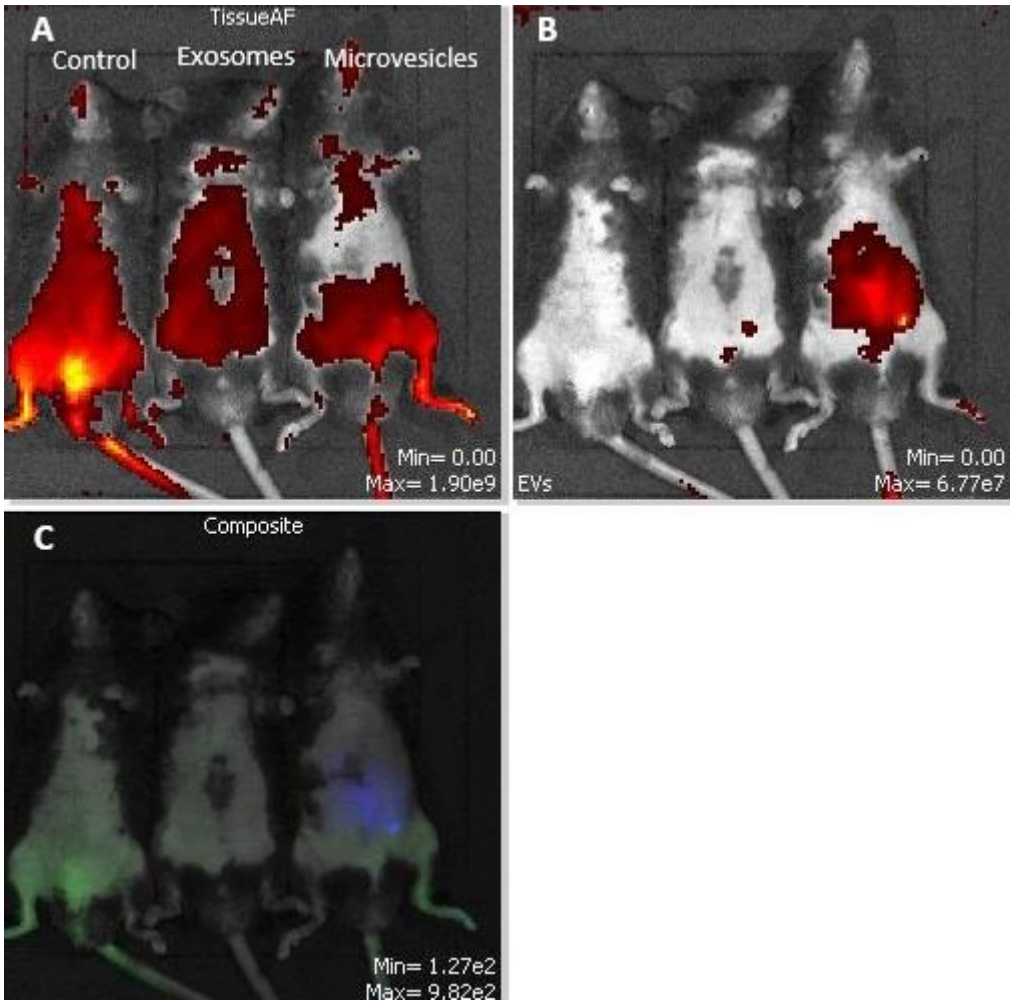

Figure 39. *In vivo* imaging to detect EVs at time points 0 after their IP administration. The Spectral Unmixing at time 0: a) tissue autofluorescence in mice, b) EVs fluorescence present in mice with exosomes and microvesicles, c) composite of both fluorescences in which green autofluorescence is noticed in control mouse and microvesicles-mouse with blue fluorescence.

Figure 40 shows the Spectral Unmixing *in vivo* at time 24 h, control mouse did not present any fluorescence, in the mouse with exosomes blue fluorescence starts to be noticed and in the one with microvesicles it is seen that the fluorescence has started to be distributed from the area of administration towards up.

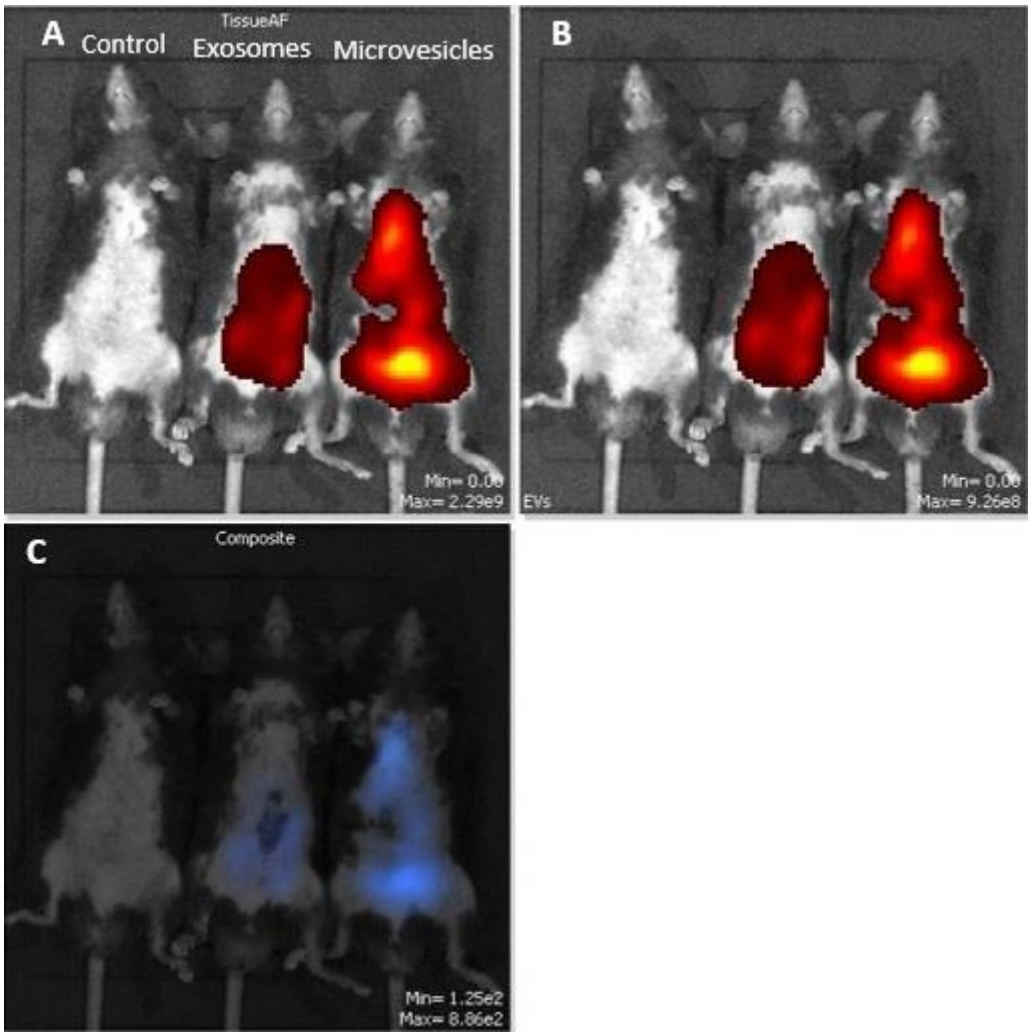

Figure 40. *In vivo* imaging to detect EVs at time points 24 h after their IP administration. The Spectral Unmixing at time 24 h: a) tissue autofluorescence in both treated mice, b) EVs fluorescence detected in both mice, c) in composite blue fluorescence more distributed in the mouse with microvesicles than the one with exosomes.

And for time 6 days in **Figure** 41, *in vivo* Spectral Unmixing shows that the fluorescence is more defined in the middle part of the mouse with exosomes while the one with microvesicles shows a greater distribution of fluorescence from the site of administration up to the heart area and mouth; the presence of fluorescence on the left side of the experimental animal was most noticeable than the right part where it is only visible in the administration area.

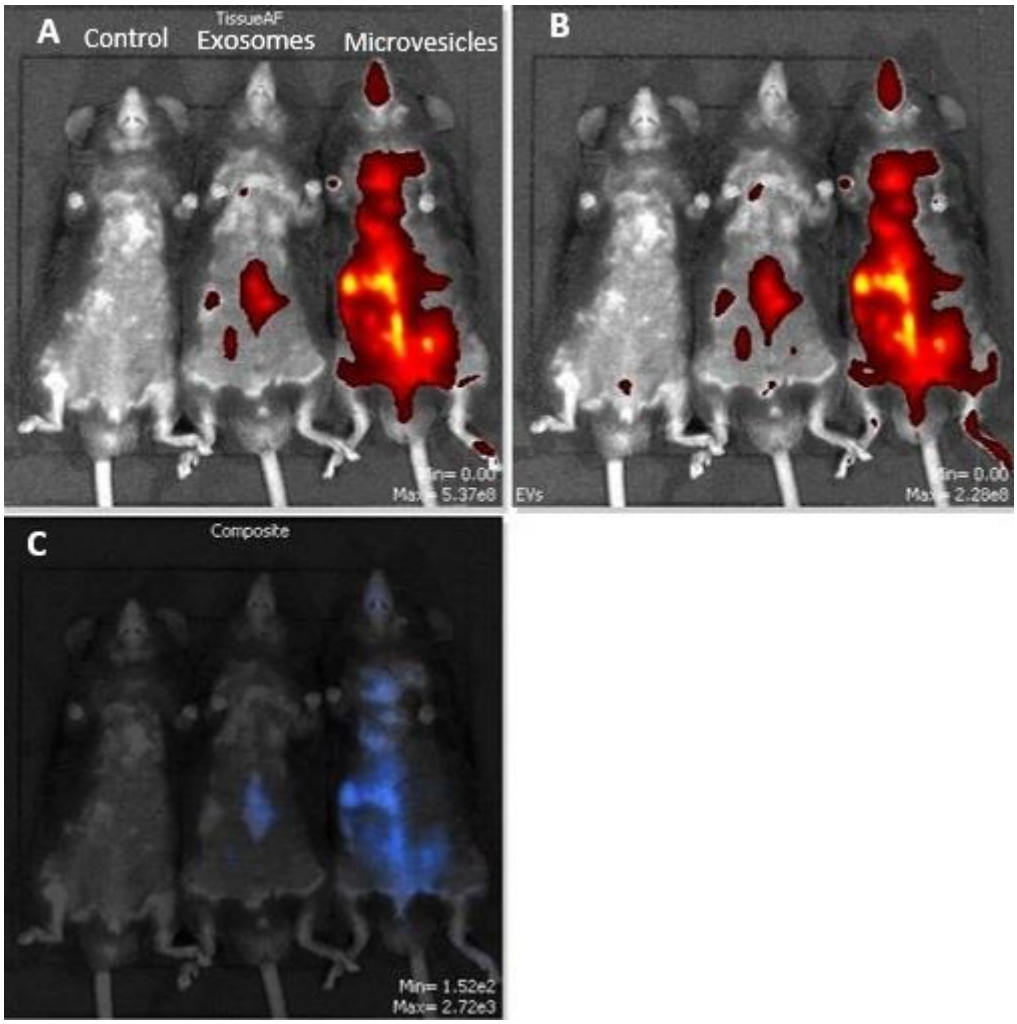

Figure 41. *In vivo* imaging to detect EVs at time points 6 days after their IP administration. The Spectral Unmixing at time 6 days: a & b) shows higher distribution in mouse with microvesicles than one with exosomes, c) the presence of microvesicles on the left side from the site of administration in the cranial direction is mainly highlighted.

Figure 42 shows *ex vivo* Spectral Unmixing, fluorescence is seen in the gut, stomach, and liver in both treated mice. In composite it is also observed lungs autofluorescence in green that corresponds to the fluorescence of the tissue.

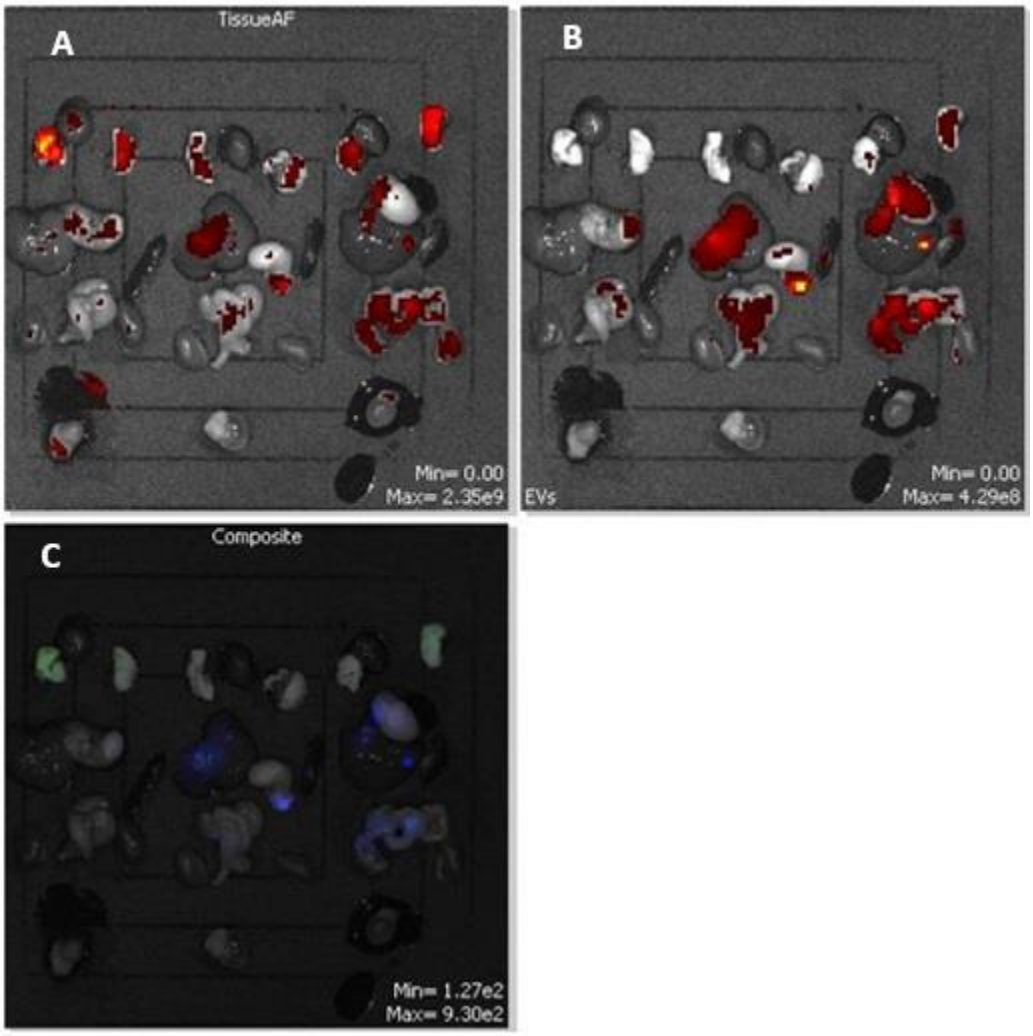

Figure 42. In vivo imaging to detect EVs ex vivo at time points 6 days after their IP administration. *Ex vivo* Spectral Unmixing: a) organs autofluorescence, b) EVs fluorescence, c) composite of both fluorescence in which green its tissue autofluorescence and in blue EVs fluorescence.

5. Discussion

CDV is one of the most impactful diseases around the world in which cardiac fibrosis appears as a common hallmark in almost all CDV (Hinderer & Schenke-Layland, 2019). Cardiac fibrosis is the pathological result of a tissue repair response to different types of tissue injury, characterize by the excessive accumulation of ECM compounds and the excessive proliferation of fibroblasts, indeed about 800,000 people die annually due to fibrotic pathologies accounting for 45% of all deaths worldwide, being cardiac and pulmonary fibrosis main accounts(Ding et al., 2020; Henderson et al., 2020; Hinderer & Schenke-Layland, 2019).

Nowadays, it is known that there is no treatment to cure cardiac fibrosis, but different diagnostic and treatment tools are currently being studied (Gyöngyösi et al., 2017; Villar et al., 2013).

In this study, we analyze a new experimental approach to reduce myocardial fibrosis, including a bio-transporter encapsulating an antifibrotic therapeutic strategy.

We have isolated, characterized and analyzed extracellular vesicles as transport vehicles for the cTPRAu-390 therapy created to decrease the expression of profibrotic genes by blocking the TFG β signaling cascade through its binding to the C-terminal Hsp90 domain (Cáceres et al., 2018; García et al., 2016).We measured protein concentration (absorbance at 280 nm) to infer the yield of each isolation. Whereas we have performed all isolations under the same conditions, we obtained a range of concentration for the EVs isolation we performed, probably depending on the final number of cells we started with. The confluence of cells varied between 75-95%.

Considering that ISEV defines large vesicles (microvesicles) as those measuring > 200 nm while small vesicles (exosomes) are those vesicles <100 nm or <200 nm, we can say that our population of both microvesicles and exosomes are within the ranges (Lamichhane et al., 2015; Théry et al., 2018) by electron microscopy detections.

Another important characteristic to be taken into account about EVs, is their charge. With Zsizer we could detect a neutral charge for microvesicles and a negative charge for exosomes population. It is known that a negative charge is normal in EVs population, also that the closer to neutral in charge the more stable they will be in circulation, charge is highly dependent on the concentration of sugar present in the membrane (de Abreu et al., 2020; Théry et al., 2018). Together with the measurements of flow cytometry, DLS was used to characterize the size of the vesicles, but reliable data could not be obtained since the size of the exosomes compared to the microvesicles was similar, considering that previously it was seen by electron microscopy that they differ in size. One reason could be that samples analyzed were placed in PBS EVs free and that samples need to be placed in a different type of buffer; other reason could be that samples used for light scattering were analyzed after 4-5 days from being isolated which could mean that EVs formed aggregates. Changes in morphology, size and composition when storing at 4°C have been already described (Théry et al., 2018).

As seen in **Figures** 19 and 20 in results section, both microvesicle and exosome populations as mentioned in the protocol by which the characterization of the EVs population was carried out, we obtained the expected population shape in EVs by flow cytometry as shown in red mark in figures already mentioned (Rotator et al., 2015).

Considering that the isolation process of EVs is long and that the storage time influences their characterization, studies on the type of storage should be carried through. Also, it should be studied how to obtain pellets that are not so dense, given the difficulty of resuspending them completely, thus leaving part of the EVs in the non-resuspended ones.

WB analysis revealed two cytosolic-proteins and one transmembrane protein presented in EVs. As shown in **Figure** 21, Flotillin-1 expression was detected in both populations microvesicles and

exosomes with non-significant difference between them. Flotillin-1 is a cytosolic protein with lipid-protein or membrane-protein binding ability, these expected marker confirms that microvesicles and exosomes have lipid bilayers capable of enclosing intracellular material. Another cytosolic protein we detected was Syntnein-1 as shown in **Figure** 22. The protein was present in both populations and with no representative difference in the amount between them. Syntenin-1 is involved in transmembrane trafficking and exosome biogenesis. Finally, CD81 protein was detected as shown in **Figure** 23, in both EVs population, with no relevant difference in the amount of protein between them. CD81 is a transmembrane protein, the presence of this marker demonstrates the specific lipid structure of the microvesicles upon bud to the plasma membrane and of the exosomes after transit of the endosomal pathway (Doyle & Wang, 2019; Ha et al., 2016; Kalra et al., 2012; Pathan et al., 2019; Théry et al., 2018; Tiwari et al., 2021). According to data obtained from vesiclepedia, Flotillin-1 has been identified 259 times and CD81 262 times in EVs (Kalra et al., 2012; Pathan et al., 2019).

After characterizing and confirming that the vesicles obtained belong to microvesicles and exosomes, the cTPRAu-390 nanocluster was encapsulated into EVs by electroporation. To confirm nanocluster encapsulation, flow cytometry technique was used to measure the percentage of cTPRau-390 encapsulated into EVs, obtaining different percentages of encapsulation.

To be used for *in vitro* experiment at 24 h and 36 h, as shown in **Table** 7, 2 electroporation pulses were applied obtaining a low percentage of encapsulation in microvesicles compared to exosomes. In the encapsulation to be used for the internalization assay, we changed the number of pulses of electroporation for microvesicles to 5 pulses given its low percentage of encapsulation and for exosomes to 3 pulses to see if there was more % of encapsulation; having that microvesicles were damaged and there was no increase in its percentage, as can be seen in the attached figures in **Appendix** 2 section, the shape of the population in flow cytometry was altered in comparison with exosomes. Finally, in the encapsulation to be used for *in vivo* experiment 2 pulses were applied, but there was not a higher encapsulation for microvesicles nor a higher change for exosomes. These results show that the number of pulses directly influences the encapsulation percentage, 2 pulses should be given to microvesicles because as it was observed in the results an increasing number of pulses to 5 led to damage to the vesicles and increasing to 3 there was no apparent difference. While for exosomes it can be said that the optimum number of pulses is 2 since increasing it to 3 showed no change (Lamichhane et al., 2015). More studies should be done on the type of encapsulation for microvesicles because although electroporation did not have a high encapsulation rate, it did have an effect on the decrease of profibrotic genes expression, so studying other methods of encapsulation for example a passive loading method as co-incubation in which the morphology of EVs is preserved so it could increase the effectiveness of this vesicle as a transport vehicle (Villata et al., 2020). In the same way, different conditions of electroporation for exosomes should be studied to see if a higher percentage of encapsulation is obtained than the one used in this work. Encapsulation methods such

as saponin treatment or hypotonic dialysis can be studied since it is known that they do not alter the constitution and functionality of the EVs (Fuhrmann et al., 2015).

As described in results section, once we encapsulated the nanocluster into EVs we proceeded to apply different treatments to NIH-3T3 cells to analyze gene expression. In the 24-hour treatment, no variation was seen in the expression of Col I, Col III or FN genes under the established conditions. While in the 36-hour treatment there was no significant difference with the non-encapsulated microvesicles treatment but there was a significant decrease in Col I, Col III and FN genes in the presence of the encapsulated therapy, whereas in the exosome treatment a greater effect in the decrease of the expression of the genes of interest was observed. What drew our attention to the exosome treatment is that in Col I, in addition to the effect of the encapsulated treatment, the non-encapsulated exosomes also had a positive effect on the decrease of expression. There was a greater decrease in the expression of Col III (** $P<0.005$) than Col I (*$P<0.05$) and FN (*$P<0.05$) compared to the controls. These results could indicate that the vehicle (EVs) could also be a therapeutic solution because is capable of reducing the expression of collagens, thus reducing fibrosis. This result is highly interesting because was additive with the presence of the antifibrotic nanocluster, providing an increase in the reduction of profibrotic genes expression.

Despite the lower amount of exosomes compared to microvesicles, there was a greater decrease in expression of the profibrotic genes but with a higher percentage of encapsulation so it may have more cTPRAu-390 than microvesicles. As we saw exosomes without therapy also decrease expression, what leads us to think that since exosomes are extracted from non-activated fibroblasts, there may be a synergistic effect in their ability to reduce gene expression, which in itself may be a better vehicle than microvesicles, because they are better encapsulated and they already have properties in their composition that help to decrease these expressions. So, it would be interesting and important to further study their composition and which components makes this expression decrease.

We can confirm that the results obtained in terms of fibrosis reduction are due to the presence of the fluorescent exogenous EVs incorporated to cells. This can be affirmed with the internalization of EVs into NIH-3T3 cells by live cell microscopy, as shown in **Figures** 28-36 in results section.

In vivo images shown that at 0 hours in exosomes mouse was non visualized distribution instead in microvesicles-mouse appeared fluorescence at the site of administration. At 24 hours the distribution of fluorescence was seen upwards towards the heart in microvesicles-mouse and exosomes- mouse started to present fluorescence; and after 6 days the distribution of the therapy from the area of administration to the mouth. It captures our attention the fact that it is mostly visualized on almost the entire left side compared to the right side in which only the injection zone is appreciated. In the *ex vivo* images, fluorescence was seen in the stomach, gut, and liver. It could mean that in the gut and stomach it is found due to the method of administration and in the liver, because it was already

degrading. What remains to be done is to extract RNA and DNA from the heart to know if the therapy reached the heart and if there was a decrease in the expression of the profibrotic genes. We should also extract RNA and DNA from the skin to know if the fluorescence observed is also due to the binding to the skin or because of our nanocluster. More *in vivo* experiments should be performed to obtain the exact time point in which EVs locate in the heart.

6. Conclusions

The protocol used for isolation has been demonstrated by EVs characterization.

The time of storage of EVs can influence in its morphology, size, and composition.

Electroporation is better encapsulation method to be used in exosomes than for microvesicles.

It is also concluded that the number of pulses in electroporation process influences in the percentage of encapsulation.

It must be said that exosomes are better vehicle transporting our therapy to treat fibrosis given the higher degree of reduction in the expression of profibrotic genes than microvesicles.

Exosomes isolated from inactivated fibroblasts are vesicles that could carry in their composition a component capable of reducing cardiac fibrosis so in addition to being used as a vehicle it could be used also as a therapy.

We have demonstrated that extracellular vesicles can be used as biological vehicles to transport potential nano-therapeutic strategies for the treatment of cardiac fibrosis given multiple advantages.

Therapies encapsulated in extracellular vesicles can be internalized into cells.

Bodipy and DiR are good dyes to stained EVs due to the fact they do not alter EVs morphology and have a good signal intensity when visualized.

EVs engineered to fluoresce can be administered *in vivo* without losing their morphology and capable of revealing their distribution.

The cTPRAu-390 nanocluster can be used as a theragnostic tool to treat cardiac fibrosis observed in NIH-3T3 cell model.

It is concluded that the sacrifice of the experimental animals after 6 days of administering this therapy turns to be a long period of time to perform the ex vivo study, since it was only possible to observe the degradation in the liver. Therefore, studies should be carried out at shorter periods to appreciate the exact moment in which the therapy reaches the heart.

Bibliography

Aires, A., Maestro, D., Ruiz del Rio, J., Palanca, A. R., Lopez-Martinez, E., Llarena, I., Geraki, K., Sanchez-Cano, C., Villar, A. V., & Cortajarena, A. L. (2021). Engineering multifunctional metal/protein hybrid nanomaterials as tools for therapeutic intervention and high-sensitivity detection. *Chemical Science*, *12*(7), 2480–2487. https://doi.org/10.1039/d0sc05215a

Akers, J. C., Gonda, D., Kim, R., Carter, B. S., & Chen, C. C. (2013). Biogenesis of extracellular vesicles (EV): Exosomes, microvesicles, retrovirus-like vesicles, and apoptotic bodies. *Journal of Neuro-Oncology*, *113*(1), 1–11. https://doi.org/10.1007/s11060-013-1084-8

Aujla, P. K., & Kassiri, Z. (2021). Diverse origins and activation of fibroblasts in cardiac fibrosis. *Cellular Signalling*, *78*, 109869. https://doi.org/10.1016/j.cellsig.2020.109869

Biernacka, A., Dobaczewski, M., & Frangogiannis, N. G. (2011). TGF-β signaling in fibrosis. *Growth Factors*, *29*(5), 196–202. https://doi.org/10.3109/08977194.2011.595714

Biernacka, A., & Frangogiannis, N. G. (2011). Aging and cardiac fibrosis. *Aging and Disease*, *2*(2), 158–173.

Boulanger, C. M., Loyer, X., Rautou, P. E., & Amabile, N. (2017). Extracellular vesicles in coronary artery disease. *Nature Reviews Cardiology*, *14*(5), 259–272. https://doi.org/10.1038/nrcardio.2017.7

Cáceres, R. A., Chavez, T., Maestro, D., Palanca, A. R., Bolado, P., Madrazo, F., Aires, A., Cortajarena, A. L., & Villar, A. V. (2018). Reduction of cardiac TGFβ-mediated profibrotic events by inhibition of Hsp90 with engineered protein. *Journal of Molecular and Cellular Cardiology*, *123*(August), 75–87. https://doi.org/10.1016/j.yjmcc.2018.08.016

Colunga Biancatelli, R. M. L., Solopov, P., Gregory, B., & Catravas, J. D. (2020). Hsp90 inhibition and modulation of the proteome: Therapeutical implications for idiopathic pulmonary fibrosis (ipf). *International Journal of Molecular Sciences*, *21*(15), 1–15. https://doi.org/10.3390/ijms21155286

Cortajarena, A. L., Wang, J., & Regan, L. (2010). Crystal structure of a designed tetratricopeptide repeat module in complex with its peptide ligand. *FEBS Journal*, *277*(4), 1058–1066. https://doi.org/10.1111/j.1742-4658.2009.07549.x

de Abreu, R. C., Fernandes, H., da Costa Martins, P. A., Sahoo, S., Emanueli, C., & Ferreira, L. (2020). Native and bioengineered extracellular vesicles for cardiovascular therapeutics. *Nature Reviews Cardiology*, *17*(11), 685–697. https://doi.org/10.1038/s41569-020-0389-5

DeLeon-Pennell, K. Y., Barker, T. H., & Lindsey, M. L. (2020). Fibroblasts: The arbiters of extracellular matrix remodeling. *Matrix Biology*, *91–92*, 1–7. https://doi.org/10.1016/j.matbio.2020.05.006

Ding, Y., Wang, Y., Jia, Q., Wang, X., Lu, Y., Zhang, A., Lv, S., & Zhang, J. (2020). Morphological and Functional Characteristics of Animal Models of Myocardial Fibrosis Induced by Pressure Overload. *International Journal of Hypertension*, *2020*. https://doi.org/10.1155/2020/3014693

Doyle, L. M., & Wang, M. Z. (2019). Overview of Extracellular Vesicles, Their Origin, Composition, Purpose, and Methods for Exosome Isolation and Analysis. *Cells*, *8*(7), 727.

El Andaloussi, S., Mäger, I., Breakefield, X. O., & Wood, M. J. A. (2013). Extracellular vesicles: Biology and emerging therapeutic opportunities. *Nature Reviews Drug Discovery*, *12*(5), 347–357. https://doi.org/10.1038/nrd3978

Fan, D., Takawale, A., Lee, J., & Kassiri, Z. (2012). Cardiac fibroblasts, fibrosis and extracellular matrix remodeling in heart disease. *Fibrogenesis and Tissue Repair*, *5*(1), 1–13. https://doi.org/10.1186/1755-1536-5-15

Fan, Z., & Guan, J. (2016). Antifibrotic therapies to control cardiac fibrosis. *Biomaterials Research*, *20*(1), 1–13. https://doi.org/10.1186/s40824-016-0060-8

Fang, L., Murphy, A. J., & Dart, A. M. (2017). A clinical perspective of anti-fibrotic therapies for cardiovascular disease. *Frontiers in Pharmacology*, *8*(APR), 1–8. https://doi.org/10.3389/fphar.2017.00186

Finnson, K. W., Almadani, Y., & Philip, A. (2020). Non-canonical (non-SMAD2/3) TGF-β signaling in fibrosis: Mechanisms and targets. *Seminars in Cell and Developmental Biology*, *101*(November), 115–122. https://doi.org/10.1016/j.semcdb.2019.11.013

Fuhrmann, G., Serio, A., Mazo, M., Nair, R., & Stevens, M. M. (2015). Active loading into extracellular vesicles significantly improves the cellular uptake and photodynamic effect of porphyrins. *Journal of Controlled Release*, *205*, 35–44. https://doi.org/10.1016/j.jconrel.2014.11.029

Gallego Muñoz, C., Saldarriaga, C. I., & Diez Martínez, J. (2019). Myocardial fibrosis: towards a new approach. *Revista Colombiana de Cardiologia*, *26*(3), 142–151. https://doi.org/10.1016/j.rccar.2018.09.006

Gandham, S., Su, X., Wood, J., Nocera, A. L., Alli, S. C., Milane, L., Zimmerman, A., Amiji, M., & Ivanov, A. R. (2020). Technologies and Standardization in Research on Extracellular Vesicles. *Trends in Biotechnology*, *38*(10), 1066–1098. https://doi.org/10.1016/j.tibtech.2020.05.012

García, R., Merino, D., Gómez, J. M., Nistal, J. F., Hurlé, M. A., Cortajarena, A. L., & Villar, A. V. (2016). Extracellular heat shock protein 90 binding to TGFβ receptor I participates in TGFβ-mediated collagen production in myocardial fibroblasts. *Cellular Signalling*, *28*(10), 1563–1579. https://doi.org/10.1016/j.cellsig.2016.07.003

Gibb, A. A., Lazaropoulos, M. P., & Elrod, J. W. (2020). Myofibroblasts and fibrosis: Mitochondrial and metabolic control of cellular differentiation. *Circulation Research*, *127*(3), 427–447. https://doi.org/10.1161/CIRCRESAHA.120.316958

Gyöngyösi, M., Winkler, J., Ramos, I., Do, Q. T., Firat, H., McDonald, K., González, A., Thum, T., Díez, J., Jaisser, F., Pizard, A., & Zannad, F. (2017). Myocardial fibrosis: biomedical research from bench to bedside. *European Journal of Heart Failure*, *19*(2), 177–191. https://doi.org/10.1002/ejhf.696

Ha, D., Yang, N., & Nadithe, V. (2016). Exosomes as therapeutic drug carriers and delivery vehicles across biological membranes: current perspectives and future challenges. *Acta Pharmaceutica Sinica B*, *6*(4), 287–296. https://doi.org/10.1016/j.apsb.2016.02.001

Henderson, N. C., Rieder, F., & Wynn, T. A. (2020). Fibrosis: from mechanisms to medicines. In *Nature* (Vol. 587, Issue 7835, pp. 555–566). https://doi.org/10.1038/s41586-020-2938-9

Hinderer, S., & Schenke-Layland, K. (2019). Cardiac fibrosis – A short review of causes and therapeutic strategies. *Advanced Drug Delivery Reviews*, *146*, 77–82. https://doi.org/10.1016/j.addr.2019.05.011

Hoter, A., El-Sabban, M. E., & Naim, H. Y. (2018). The HSP90 family: Structure, regulation, function, and implications in health and disease. *International Journal of Molecular Sciences*, *19*(9). https://doi.org/10.3390/ijms19092560

Janas, T., Janas, M. M., Sapoń, K., & Janas, T. (2015). Mechanisms of RNA loading into exosomes. *FEBS Letters*, *589*(13), 1391–1398. https://doi.org/10.1016/j.febslet.2015.04.036

Kalra, H., Drummen, G. P. C., & Mathivanan, S. (2016). Focus on extracellular vesicles: Introducing the next small big thing. *International Journal of Molecular Sciences*, *17*(2). https://doi.org/10.3390/ijms17020170

Kalra, H., Simpson, R. J., Ji, H., Aikawa, E., Altevogt, P., Askenase, P., Bond, V. C., Borràs, F. E.,

Breakefield, X., Budnik, V., Buzas, E., Camussi, G., Clayton, A., Cocucci, E., Falcon-Perez, J. M., Gabrielsson, S., Gho, Y. S., Gupta, D., Harsha, H. C., … Mathivanan, S. (2012). Vesiclepedia: A Compendium for Extracellular Vesicles with Continuous Community Annotation. *PLoS Biology*, *10*(12), 8–12. https://doi.org/10.1371/journal.pbio.1001450

Kong, P., Christia, P., & Frangogiannis, N. G. (2014). The pathogenesis of cardiac fibrosis. *Cellular and Molecular Life Sciences*, *71*(4), 549–574. https://doi.org/10.1007/s00018-013-1349-6

Lamichhane, T. N., Raiker, R. S., & Jay, S. M. (2015). Exogenous DNA loading into extracellular vesicles via electroporation is size-dependent and enables limited gene delivery. *Molecular Pharmaceutics*, *12*(10), 3650–3657. https://doi.org/10.1021/acs.molpharmaceut.5b00364

Lawson, C., Vicencio, J. M., Yellon, D. M., & Davidson, S. M. (2016). Microvesicles and exosomes: New players in metabolic and cardiovascular disease. *Journal of Endocrinology*, *228*(2), R57–R71. https://doi.org/10.1530/JOE-15-0201

Leask, A. (2007). TGFβ, cardiac fibroblasts, and the fibrotic response. *Cardiovascular Research*, *74*(2), 207–212. https://doi.org/10.1016/j.cardiores.2006.07.012

Leask, A. (2015). Getting to the heart of the matter: New insights into cardiac fibrosis. *Circulation Research*, *116*(7), 1269–1276. https://doi.org/10.1161/CIRCRESAHA.116.305381

Liu, G., Ma, C., Yang, H., & Zhang, P. Y. (2017). Transforming growth factor β and its role in heart disease. *Experimental and Therapeutic Medicine*, *13*(5), 2123–2128. https://doi.org/10.3892/etm.2017.4246

Lu, L., Guo, J., Hua, Y., Huang, K., Magaye, R., Cornell, J., Kelly, D. J., Reid, C., Liew, D., Zhou, Y., Chen, A., Xiao, W., Fu, Q., & Wang, B. H. (2017). Cardiac fibrosis in the ageing heart: Contributors and mechanisms. *Clinical and Experimental Pharmacology and Physiology*, *44*(November 2016), 55–63. https://doi.org/10.1111/1440-1681.12753

Ma, Z. G., Yuan, Y. P., Wu, H. M., Zhang, X., & Tang, Q. Z. (2018). Cardiac fibrosis: New insights into the pathogenesis. *International Journal of Biological Sciences*, *14*(12), 1645–1657. https://doi.org/10.7150/ijbs.28103

Marinova, M., Solopov, P., Dimitropoulou, C., Colunga Biancatelli, R. M. L., & Catravas, J. D. (2020). Post-treatment with a heat shock protein 90 inhibitor prevents chronic lung injury and pulmonary fibrosis, following acute exposure of mice to HCl. *Experimental Lung Research*, *46*(6), 203–216. https://doi.org/10.1080/01902148.2020.1764148

Melzer, M., Beier, D., Young, P. P., & Saraswati, S. (2020). Isolation and characterization of adult cardiac fibroblasts and myofibroblasts. *Journal of Visualized Experiments*, *2020*(157), 1–11. https://doi.org/10.3791/60909

Murtha, L. A., Schuliga, M. J., Mabotuwana, N. S., Hardy, S. A., Waters, D. W., Burgess, J. K., Knight, D. A., & Boyle, A. J. (2017). The processes and mechanisms of cardiac and pulmonary fibrosis. *Frontiers in Physiology*, *8*(OCT), 1–15. https://doi.org/10.3389/fphys.2017.00777

Nandi, S. S., & Mishra, P. K. (2015). Harnessing fetal and adult genetic reprograming for therapy of heart disease. *Journal of Nature and Science*, *1*(4). http://www.ncbi.nlm.nih.gov/pubmed/25879081%0Ahttp://www.pubmedcentral.nih.gov/articlerender.fcgi?artid=PMC4394627

Parichatikanond, W., Luangmonkong, T., Mangmool, S., & Kurose, H. (2020). Therapeutic targets for the treatment of cardiac fibrosis and cancer: Focusing on tgf-β Signaling. *Frontiers in Cardiovascular Medicine*, *7*(March), 1–19. https://doi.org/10.3389/fcvm.2020.00034

Pathan, M., Fonseka, P., Chitti, S. V., Kang, T., Sanwlani, R., Van Deun, J., Hendrix, A., & Mathivanan, S. (2019). Vesiclepedia 2019: A compendium of RNA, proteins, lipids and metabolites in extracellular vesicles. *Nucleic Acids Research*, *47*(D1), D516–D519. https://doi.org/10.1093/nar/gky1029

Perez-Riba, A., & Itzhaki, L. S. (2019). The tetratricopeptide-repeat motif is a versatile platform that enables diverse modes of molecular recognition. *Current Opinion in Structural Biology*, *54*, 43–49. https://doi.org/10.1016/j.sbi.2018.12.004

Ranjan, P., Kumari, R., & Verma, S. K. (2019). Cardiac Fibroblasts and Cardiac Fibrosis: Precise Role of Exosomes. *Frontiers in Cell and Developmental Biology*, *7*(December), 1–12. https://doi.org/10.3389/fcell.2019.00318

Rotator, T., Exosome, C., & Igg, M. (2015). *Characterization of exosomes*. *March*, 2–3.

Sluijter, J. P. G., Verhage, V., Deddens, J. C., Van Den Akker, F., & Doevendans, P. A. (2014). Microvesicles and exosomes for intracardiac communication. *Cardiovascular Research*, *102*(2), 302–311. https://doi.org/10.1093/cvr/cvu022

Solopov, P., Marinova, M., Dimitropoulou, C., & Catravas, J. D. (2019). *Heat Shock Protein (HSP) 90 Inhibitors Prevent the Development of Nitrogen Mustard-Induced Chronic Lung Injury and Pulmonary Fibrosis in Mice*. *Level 3*, A1021–A1021. https://doi.org/10.1164/ajrccm-conference.2019.199.1_meetingabstracts.a1021

Talman, V., & Ruskoaho, H. (2016). Cardiac fibrosis in myocardial infarction—from repair and remodeling to regeneration. *Cell and Tissue Research*, *365*(3), 563–581. https://doi.org/10.1007/s00441-016-2431-9

Théry, C., Witwer, K. W., Aikawa, E., Alcaraz, M. J., Anderson, J. D., Andriantsitohaina, R., Antoniou, A., Arab, T., Archer, F., Atkin-Smith, G. K., Ayre, D. C., Bach, J. M., Bachurski, D., Baharvand, H., Balaj, L., Baldacchino, S., Bauer, N. N., Baxter, A. A., Bebawy, M., … Zuba-Surma, E. K. (2018). Minimal information for studies of extracellular vesicles 2018 (MISEV2018): a position statement of the International Society for Extracellular Vesicles and update of the MISEV2014 guidelines. *Journal of Extracellular Vesicles*, *7*(1). https://doi.org/10.1080/20013078.2018.1535750

Tian, J., An, X., & Niu, L. (2017). Myocardial fibrosis in congenital and pediatric heart disease (Review). *Experimental and Therapeutic Medicine*, *13*(5), 1660–1664. https://doi.org/10.3892/etm.2017.4224

Tiwari, S., Kumar, V., Randhawa, S., & Verma, S. K. (2021). Preparation and characterization of extracellular vesicles. In *American Journal of Reproductive Immunology* (Vol. 85, Issue 2). https://doi.org/10.1111/aji.13367

Tkach, M., & Théry, C. (2016). Communication by Extracellular Vesicles: Where We Are and Where We Need to Go. *Cell*, *164*(6), 1226–1232. https://doi.org/10.1016/j.cell.2016.01.043

Tomcik, M., Zerr, P., Pitkowski, J., Palumbo-Zerr, K., Avouac, J., Distler, O., Becvar, R., Senolt, L., Schett, G., & Distler, J. H. (2014). Heat shock protein 90 (Hsp90) inhibition targets canonical TGF-β signalling to prevent fibrosis. *Annals of the Rheumatic Diseases*, *73*(6), 1215–1222. https://doi.org/10.1136/annrheumdis-2012-203095

Travers, J. G., Kamal, F. A., Robbins, J., Yutzey, K. E., & Blaxall, B. C. (2016). Cardiac fibrosis: The fibroblast awakens. *Circulation Research*, *118*(6), 1021–1040. https://doi.org/10.1161/CIRCRESAHA.115.306565

Van Dommelen, S. M., Vader, P., Lakhal, S., Kooijmans, S. A. A., Van Solinge, W. W., Wood, M. J. A., & Schiffelers, R. M. (2012). Microvesicles and exosomes: Opportunities for cell-derived membrane vesicles in drug delivery. *Journal of Controlled Release*, *161*(2), 635–644. https://doi.org/10.1016/j.jconrel.2011.11.021

Van Niel, G., D'Angelo, G., & Raposo, G. (2018). Shedding light on the cell biology of extracellular vesicles. *Nature Reviews Molecular Cell Biology*, *19*(4), 213–228. https://doi.org/10.1038/nrm.2017.125

Villar, A. V., García, R., Llano, M., Cobo, M., Merino, D., Lantero, A., Tramullas, M., Hurlé, J. M.,

Hurlé, M. A., & Nistal, J. F. (2013). BAMBI (BMP and activin membrane-bound inhibitor) protects the murine heart from pressure-overload biomechanical stress by restraining TGF-β signaling. *Biochimica et Biophysica Acta - Molecular Basis of Disease*, *1832*(2), 323–335. https://doi.org/10.1016/j.bbadis.2012.11.007

Villata, S., Canta, M., & Cauda, V. (2020). Evs and bioengineering: From cellular products to engineered nanomachines. *International Journal of Molecular Sciences*, *21*(17), 1–32. https://doi.org/10.3390/ijms21176048

Wrighton, K. H., Lin, X., & Feng, X. H. (2008). Critical regulation of TGFβ signaling by Hsp90. *Proceedings of the National Academy of Sciences of the United States of America*, *105*(27), 9244–9249. https://doi.org/10.1073/pnas.0800163105

Yáñez-Mó, M., Siljander, P. R. M., Andreu, Z., Zavec, A. B., Borràs, F. E., Buzas, E. I., Buzas, K., Casal, E., Cappello, F., Carvalho, J., Colás, E., Cordeiro-Da Silva, A., Fais, S., Falcon-Perez, J. M., Ghobrial, I. M., Giebel, B., Gimona, M., Graner, M., Gursel, I., … De Wever, O. (2015). Biological properties of extracellular vesicles and their physiological functions. *Journal of Extracellular Vesicles*, *4*(2015), 1–60. https://doi.org/10.3402/jev.v4.27066

Yousefi, F., Shabaninejad, Z., Vakili, S., Derakhshan, M., Movahedpour, A., Dabiri, H., Ghasemi, Y., Mahjoubin-Tehran, M., Nikoozadeh, A., Savardashtaki, A., Mirzaei, H., & Hamblin, M. R. (2020). TGF-β and WNT signaling pathways in cardiac fibrosis: Non-coding RNAs come into focus. *Cell Communication and Signaling*, *18*(1), 1–16. https://doi.org/10.1186/s12964-020-00555-4

Zaborowski, M. P., Balaj, L., Breakefield, X. O., & Lai, C. P. (2015). Extracellular Vesicles: Composition, Biological Relevance, and Methods of Study. *BioScience*, *65*(8), 783–797. https://doi.org/10.1093/biosci/biv084

Zhang, X., Zhang, X., Huang, W., & Ge, X. (2021). The role of heat shock proteins in the regulation of fibrotic diseases. *Biomedicine and Pharmacotherapy*, *135*, 111067. https://doi.org/10.1016/j.biopha.2020.111067

Zhang, Y., Liu, Y., Liu, H., & Tang, W. H. (2019). Exosomes: Biogenesis, biologic function and clinical potential. *Cell and Bioscience*, *9*(1), 1–18. https://doi.org/10.1186/s13578-019-0282-2

Appendixes

Appendix 1. TEM

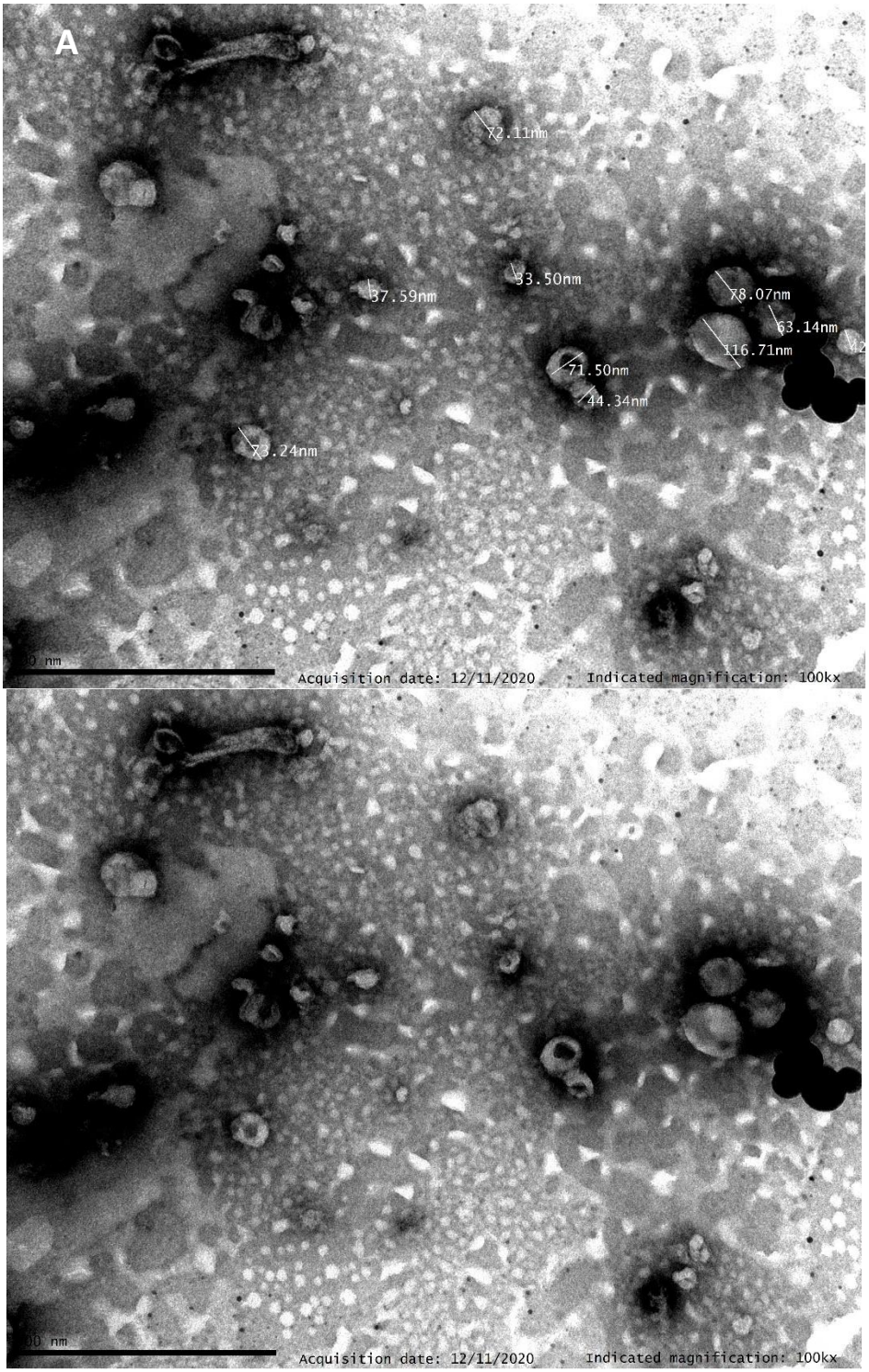

Appendix 1.1. Microvesicles visualized by electron microscopy. a) different diameter sizes, b) microvesicles without their diameter to visualized better their shape.

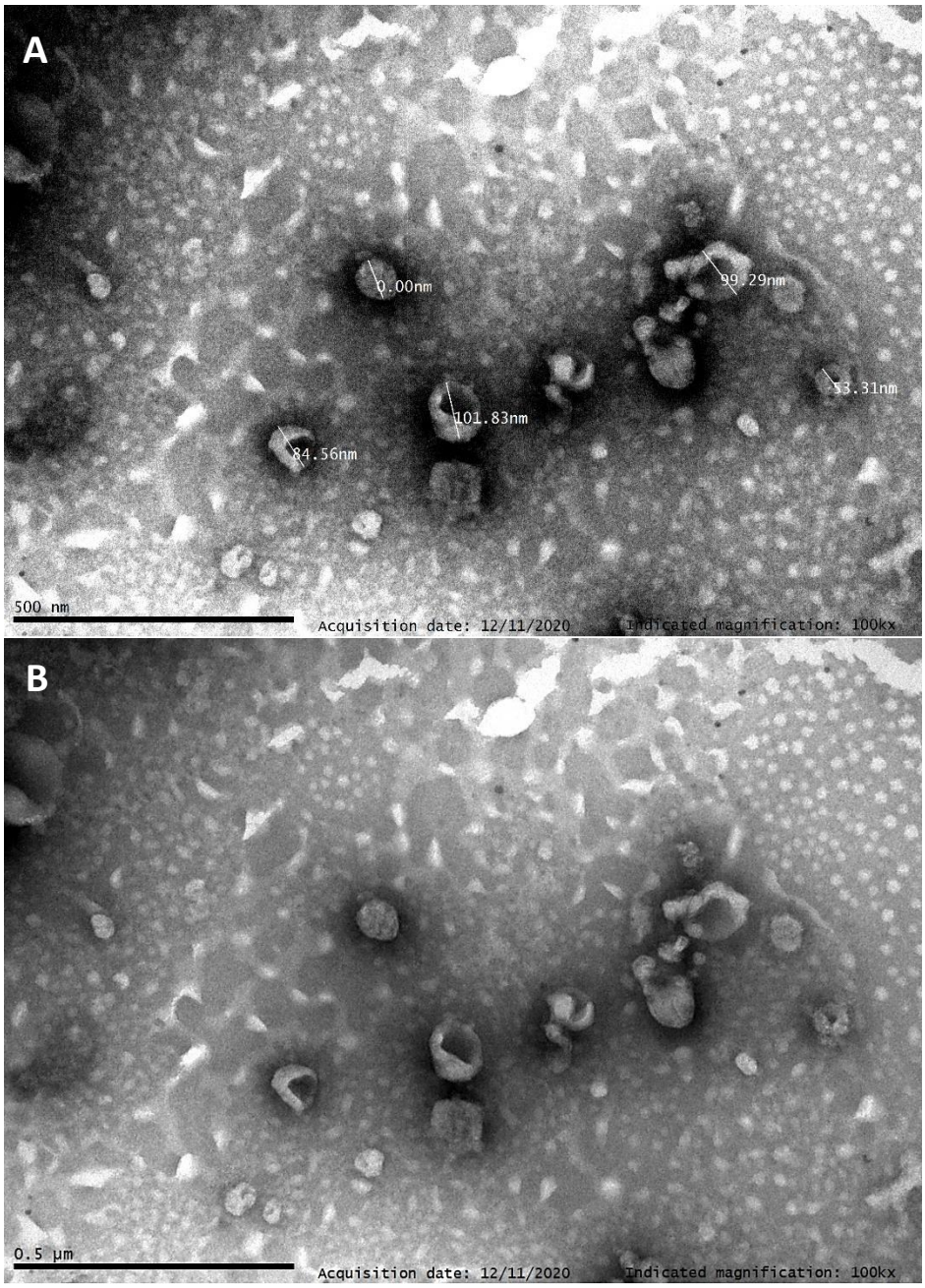

Appendix 1.2. Exosomes visualized by electron microscopy. a) different diameter sizes, b) exosomes without their diameter to visualized better their shape.

Appendix 2. Flow cytometry

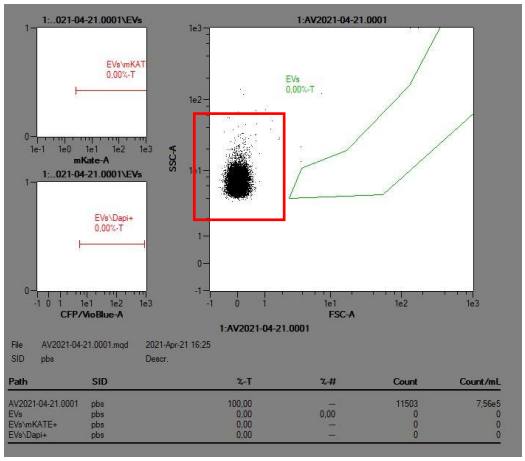

Path	SID	%-T	%-#	Count	Count/mL
AV2021-04-21.0001	pbs	100,00	---	11503	7,56e5
EVs	pbs	0,00	0,00	0	0
EVs\mKATE+	pbs	0,00	---	0	0
EVs\Dapi+	pbs	0,00	---	0	0

Appendix 2.1. PBS EVs free used as control to characterize EVs population, red mark region aside from EVs region.

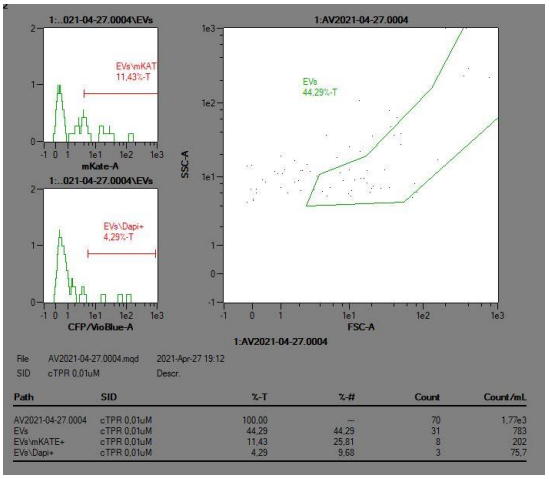

Path	SID	%-T	%-#	Count	Count/mL
AV2021-04-27.0004	cTPR 0,01uM	100,00	---	70	1,77e3
EVs	cTPR 0,01uM	44,29	44,29	31	783
EVs\mKATE+	cTPR 0,01uM	11,43	25,81	8	202
EVs\Dapi+	cTPR 0,01uM	4,29	9,68	3	75,7

Appendix 2.2. cTPRAu-390 control analyzed to confirm that it is free of EVs used in 24 and 36 h experiment.

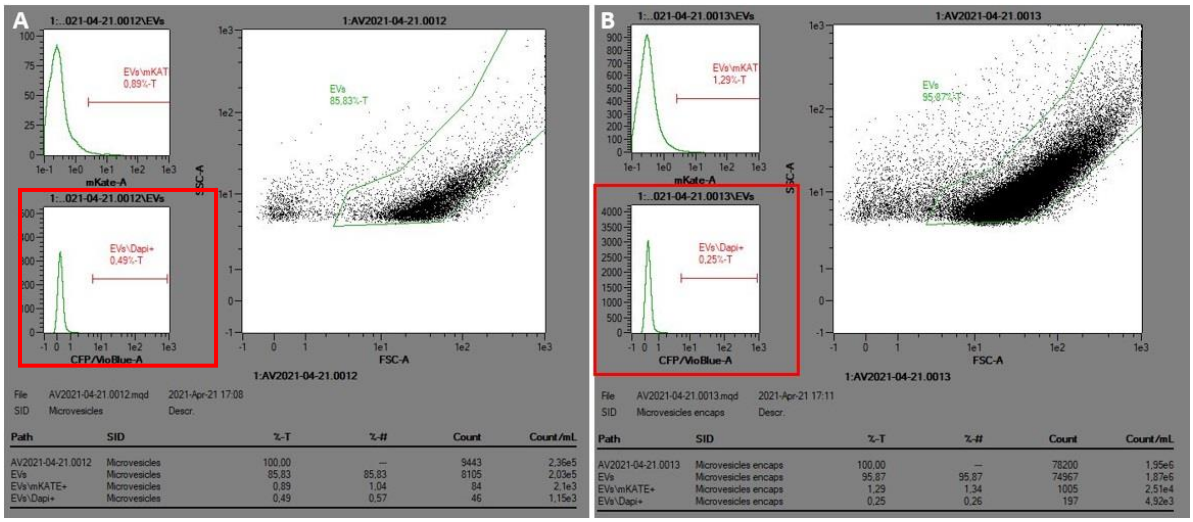

Path	SID	%-T	%-#	Count	Count/mL
AV2021-04-21.0012	Microvesicles	100,00	---	9443	2,36e5
EVs	Microvesicles	85,83	85,83	8105	2,03e5
EVs\mKATE+	Microvesicles	0,89	1,04	84	2,1e3
EVs\Dapi+	Microvesicles	0,49	0,57	46	1,15e3

Path	SID	%-T	%-#	Count	Count/mL
AV2021-04-21.0013	Microvesicles encaps	100,00	---	78200	1,95e6
EVs	Microvesicles encaps	95,87	95,87	74967	1,87e6
EVs\mKATE+	Microvesicles encaps	1,29	1,34	1005	2,51e4
EVs\Dapi+	Microvesicles encaps	0,25	0,26	197	4,92e3

Appendix 3. ctPRAu-390 encapsulation into microvesicles for 24h treatment. On the left side red region refers to% of non-encapsulated microvesicles used as control to be compared to right side red mark which represents 0.25 % of nanocluster encapsulated into microvesicles.

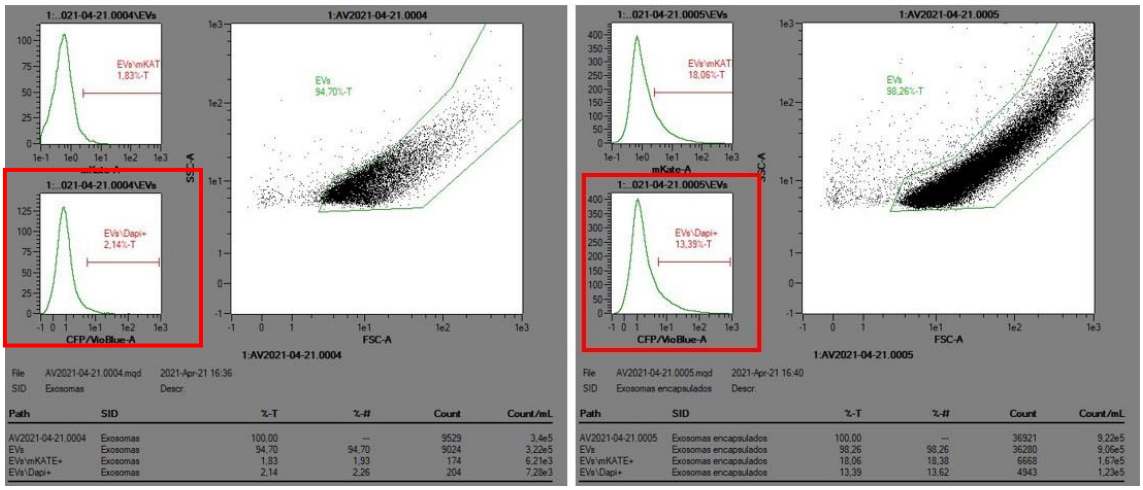

Appendix 2.3. ctPRAu-390 encapsulation into microvesicles for 24h treatment. On the left side red region refers to % of non-encapsulated exosomes used as control to be compared to right side red mark which represents 13.39 % of nanocluster encapsulated into exosomes.

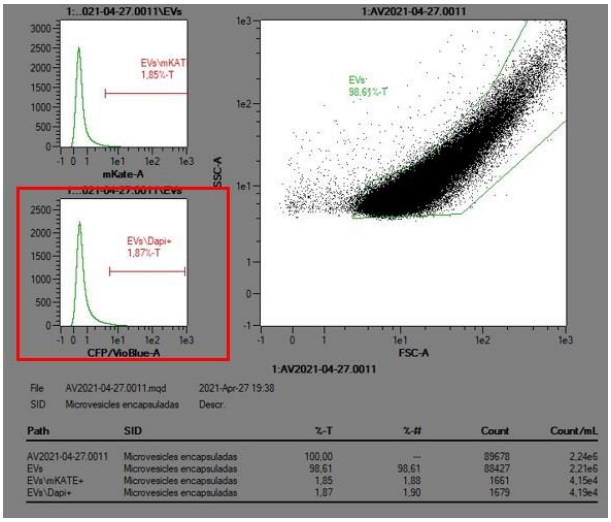

Appendix 2.4. ctPRAu-390 encapsulation into microvesicles to be used in 36h treatment. Red region refers to 1.87 % of nanocluster encapsulated into microvesicles.

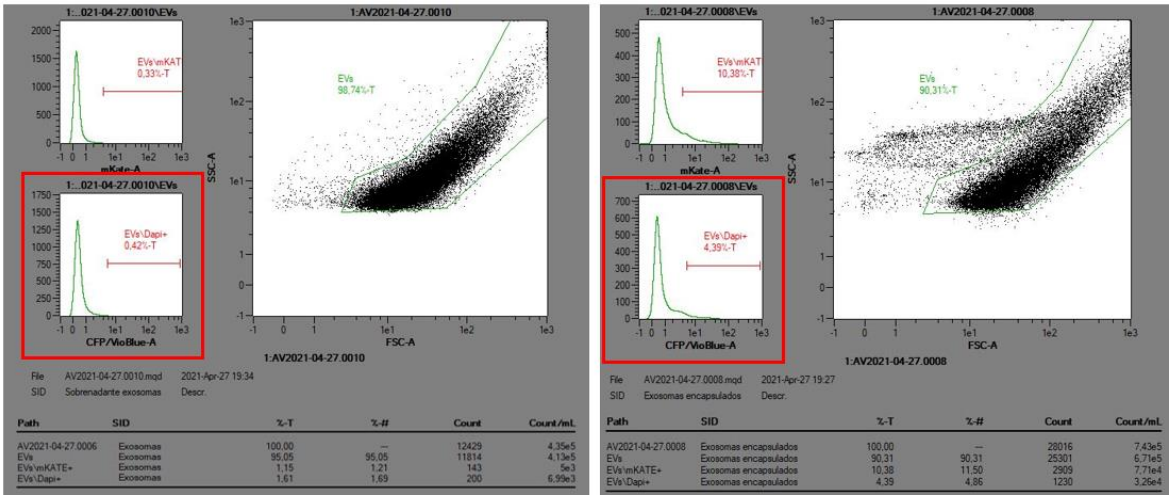

Appendix 2.5. ctPRAu-390 encapsulation into exosomes for 36h treatment. On the left side red region refers to % of non-encapsulated exosomes used as control to be compared to right side red mark which represents 4.39 % of nanocluster encapsulated into exosomes.

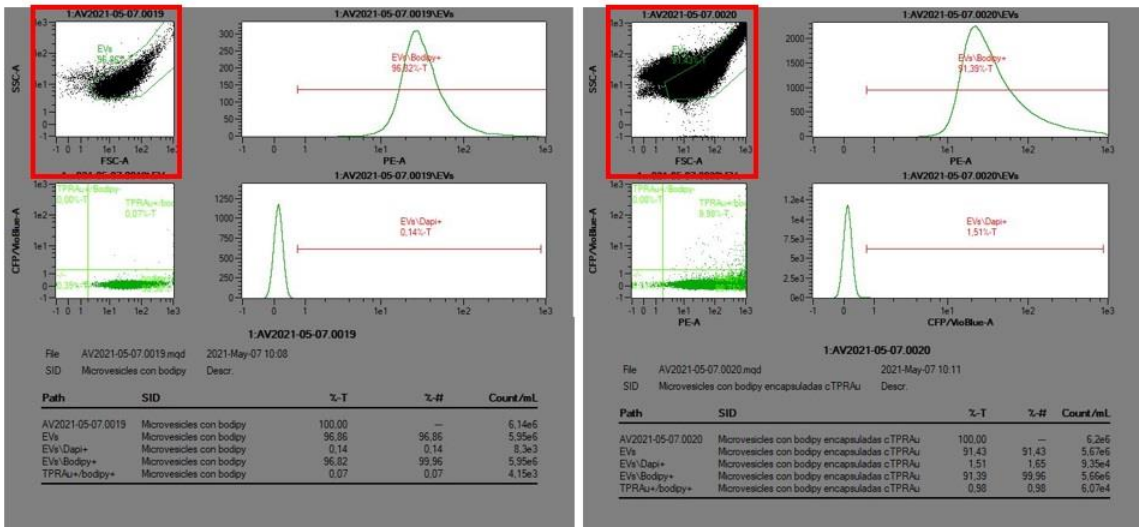

Appendix 2.6. cTPRAu-390 encapsulation into microvesicles to be use in internalization experiment. On the left side, the area marked in red represents the normal region shape of microvesicles while on the right side is an altered form due to 5 pulses given in the electroporation given a 0.98% of encapsulation.

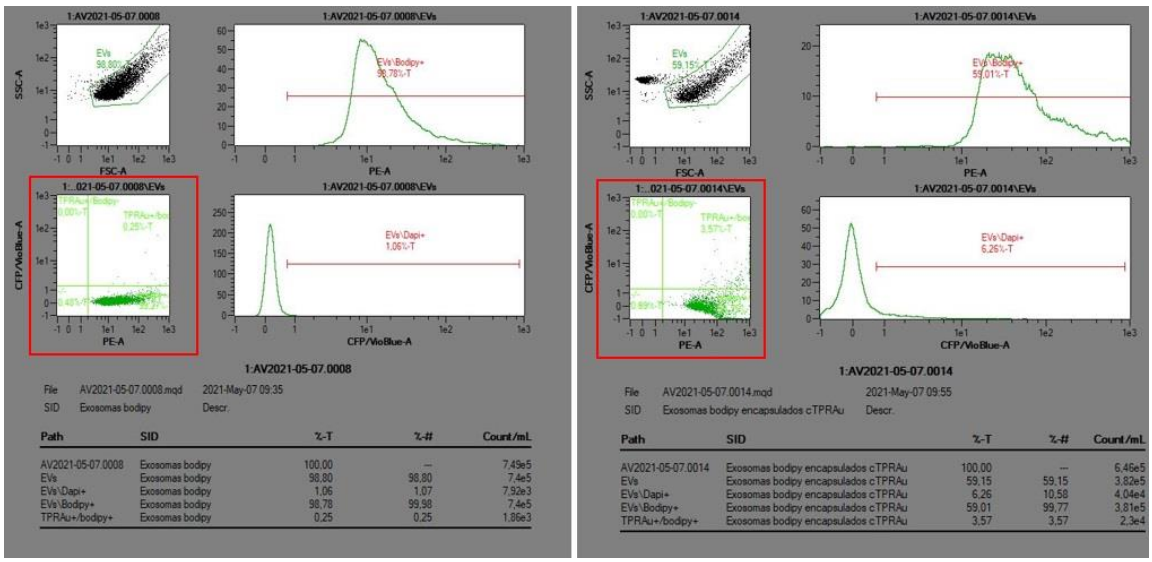

Appendix 2.7. cTPRAu-390 encapsulation into exosomes to be used in internalization experiment. On the left side, the area marked in red represents 3.57 % of nanocluster encapsulated into exosomes stained with bodipy.

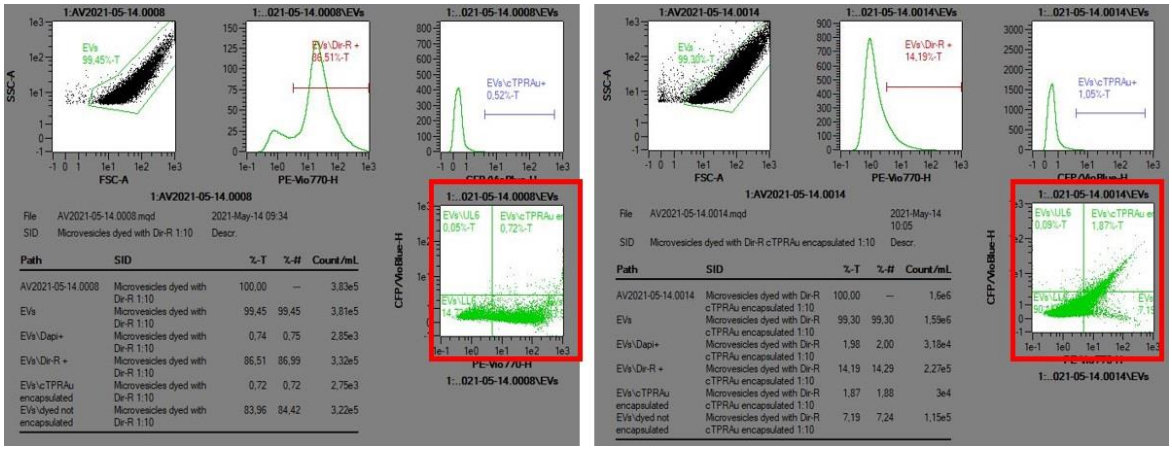

Appendix 2.8. ctPRAu-390 encapsulation into microvesicles stained with DiR to be used *in vivo* experiment. On the left side red region refers to % of non-encapsulated microvesicles used as control to be compared to right side red mark which represents 1.87 % of nanocluster encapsulated into microvesicles stained with DiR.

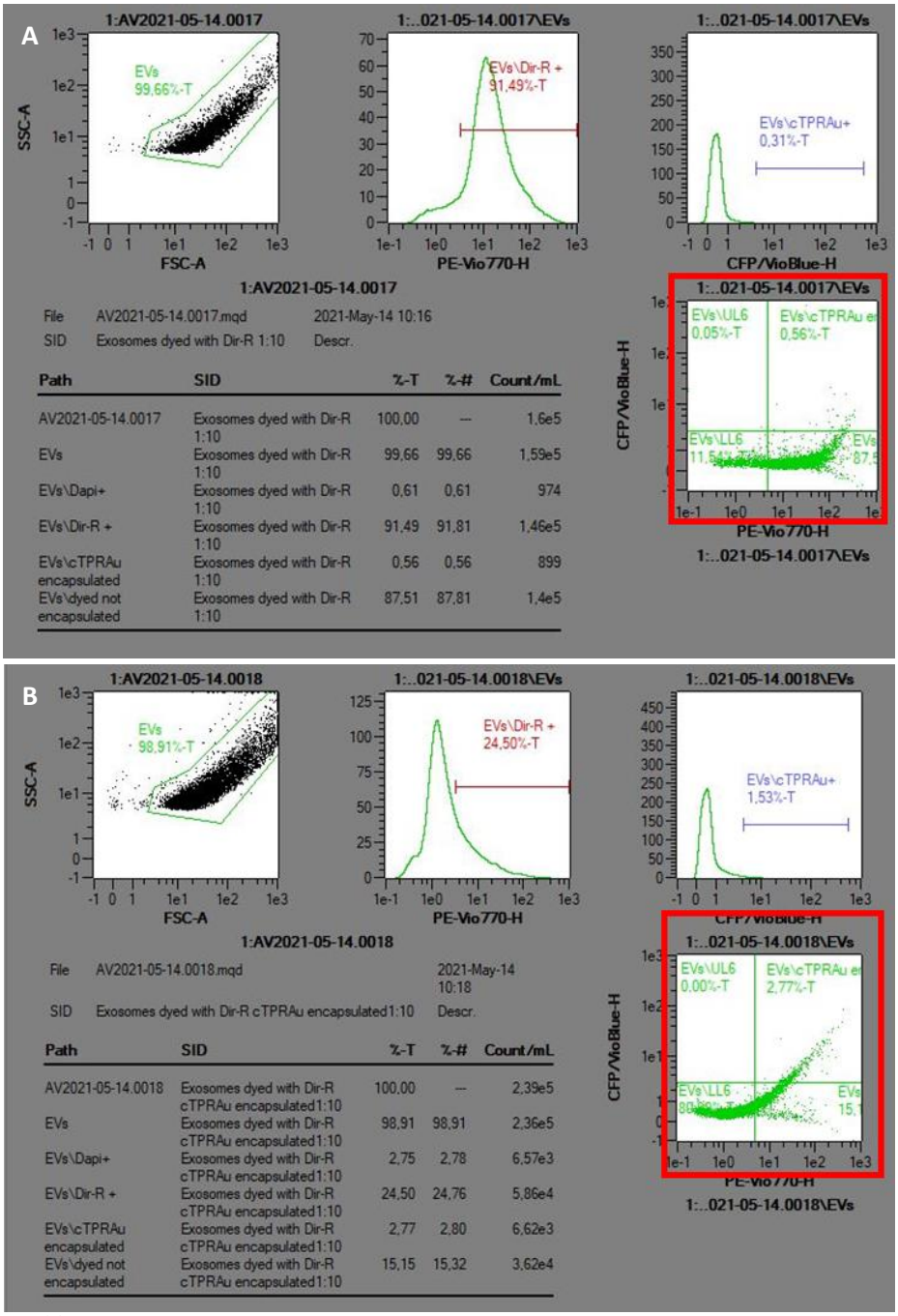

Appendix2.9. cTPRAu-390 encapsulation into exosomes stained with DiR to be used at *in vivo* experiment. a) red mark region refers to % of non-encapsulated exosomes used as control to be compared to b) red mark which represents 2.77 % of nanocluster encapsulated into exosomes stained with DiR dye.

Appendix 3. *In vivo* spectral unmixing

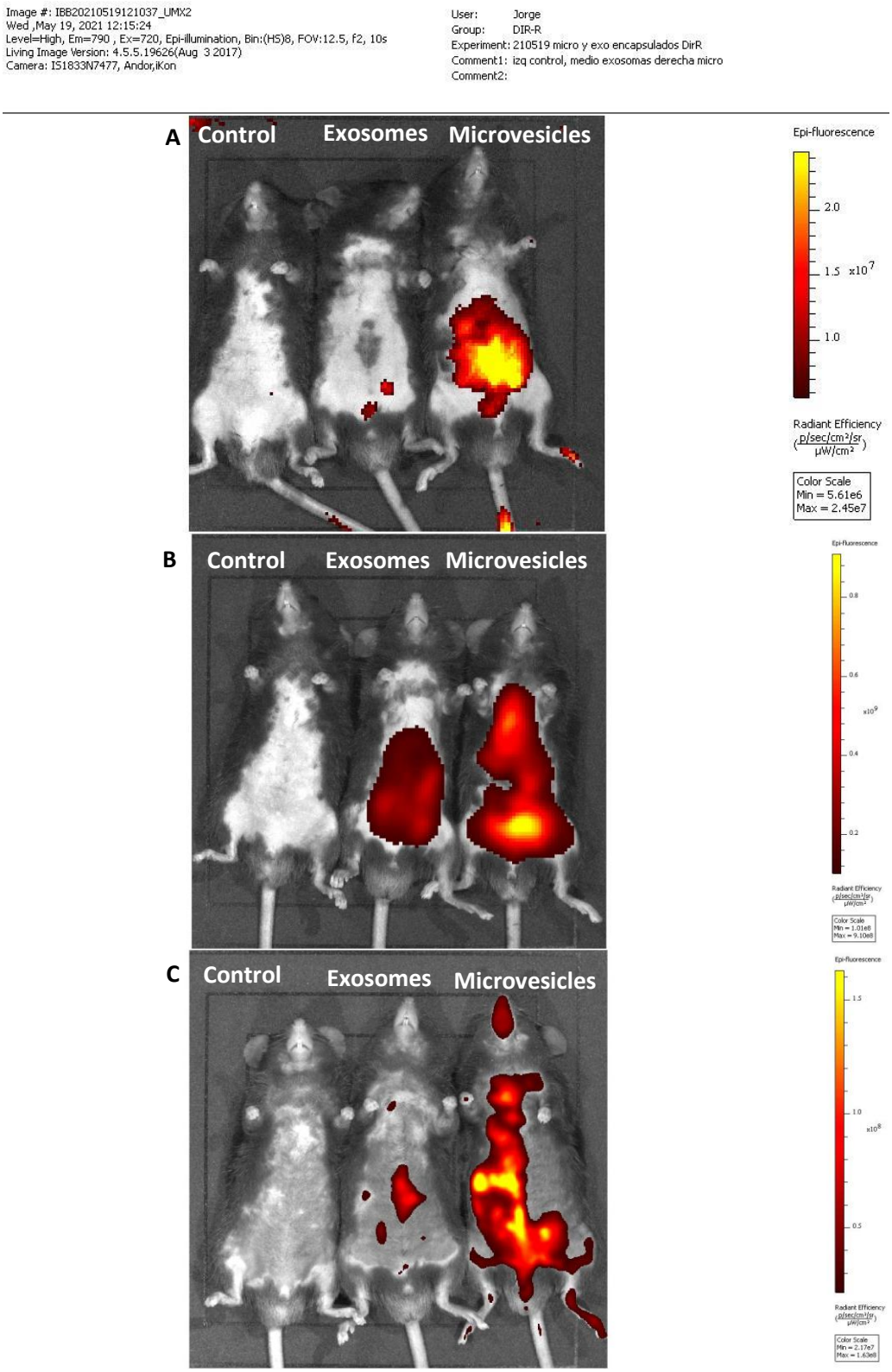

Appendix3.1. Spectral unmixing: control mice at the left doesn't present fluorescence at any time, a) t=0 h exosome-mouse with fluorescence at site of administration and microvesicle-mouse fluorescence in the lower part; b) t=24 h presence of fluorescence at lower part of exosome-mouse and a distribution of fluorescence up towards in microvesicle-mouse; c) t= 6 days fluorescence is more defined in the lower part of exosome-mouse and more defined fluorescence distributed in the upper part up to its mouth in microvesicle mouse.